copy 1

SURVEYS IN PREPARATION FOR THE COMMISSIONING OF THE TRIUMF MAGNET

by

ROBERT A. GIBB

B.Sc., UNIVERSITY OF WINDSOR, 1970

A thesis submitted in partial fulfilment of
the requirements for the degree of

Master of Science

in the Department

of

Physics

We accept this thesis as conforming to the
required standard

THE UNIVERSITY OF BRITISH COLUMBIA

December, 1972

In presenting this thesis in partial fulfilment of the requirements for an advanced degree at the University of British Columbia, I agree that the Library shall make it freely available for reference and study. I further agree that permission for extensive copying of this thesis for scholarly purposes may be granted by the Head of my Department or by his representatives. It is understood that copying or publication of this thesis for financial gain shall not be allowed without my written permission.

Department of Physics

The University of British Columbia
Vancouver 8, Canada

Date January 18,1973

ABSTRACT

This thesis was concerned with work in preparation for the commissioning of the TRIUMF cyclotron magnet. The experiments were centred around a 1/10 scale model of the cyclotron magnet. Computer calculation and model measurements were made of a model combination magnet. Extraction fields of the cyclotron were measured and the stripping foil locus determined. The interaction of the cyclotron magnet and the combination magnet was determined.

A 1/10 scale model Triple Hall Probe was constructed and precisely calibrated. Its performance was tested and surveys made in the model.

Finally the characteristics of the trim coils to be used in the cyclotron were measured.

TABLE OF CONTENTS

LIST OF TABLES

LIST OF FIGURES

ACKNOWLEDGEMENTS

I am greatly indebted to Dr. E.G. Auld for his assistance in guiding this research.

My thanks also goes to Dr. G.H. MacKenzie for his guidance in the T.H.P. work, and Dr. L. Robertson and Mr. P. Alexander for their analysis of the extraction survey data, and to A.J. Otter in the combination magnet study.

I am much indebted to the staff of the TRIUMF magnet group, namely N. Rehlinger, K. Poon, D. Evans and T. Mitchel.

1. INTRODUCTION

The TRIUMF cyclotron[1] has a six sector magnet with spiral shaped pole pieces to contain the H^- ion beam. These particles will be accelerated up to 500 Mev. but a beam having an energy from 150 Mev. or more may be extracted.[2] This is possible because the beam is extracted by placing a stripping foil in the path of the beam. The foil removes the two electrons from the ion causing a change in the charge of the beam which results in the particles spiralling out of the machine. Since the energy of the beam is a function of radius and azimuth, then the position of the stripping foil for each energy of extraction is a function of radius and azimuth.

Beams of each energy must travel through a 'horn' in the vacuum tank of the cyclotron. This horn projects out between the return yokes of two adjacent pole pieces. To bend the beam into the transport system, a combination magnet will be provided that can accept beams of all the possible energies and deflect them a suitable amount. Also the dispersion of the beam as it travels through this system must be minimized.

To provide the focusing and isochronism necessary, the field of the magnet can be adjusted by bolting shims[3] to the edge of the pole pieces of each sector. This

step must be done before the magnet is put into operation. To make small changes in the beam orbits during operation a system of trim and harmonic coils are provided. The trim coils are circular, with the cyclotron centre as their centre; they can change the average field. There is also a set of harmonic coils for each pole; these can change the field under a given pole piece as a function of radius.

An important property of the field is its variation in the vertical direction about the geometric median plane. The ideal is a field symmetric about this plane and which varies slowly about this surface. A knowledge of the deviations from this ideal condition that exist is important since it affects the vertical motion of the particle beam.[4]

In the following chapters I shall present studies made of these features of the magnets associated with the operation of the TRIUMF cyclotron. A 1/10 scale model of the cyclotron magnet is the chief facility for this work. In addition the magnet lab is equipped with a calibration magnet and an NMR digital gaussmeter for the calibration of probes. A Hewelett Packard 2116B with a 16k core and two 9 track tape drives provide the data acquisition capabilities and some computing power for this work.

2. THE TRIM PROGRAM AND THE COMBINATION MAGNET

2.1 TRIM Program

TRIM is a two dimensional relaxation program first developed at the Lawrence Radiation Laboratory, University of California[5] for the mapping of magnetic fields. A version adopted for an IBM 360/75 was obtained from the Rutherford Laboratory[6] by Paul Reeves of the University of Victoria, and this version was used on the 360/67 at the University of British Columbia. This program uses an array of triangles that are bent and moved to fit any geometry specified by the designer. Fig. 2.1 shows a typical logical diagram that can be used to find the field for an H magnet. To save computing cost the fact there are 2 planes of symmetry in such a magnet can be exploited by specifying suitable boundary conditions. Setting the vector potential to zero means there is no flux leakage across the boundary and making it reflecting means the flux lines are perpendicular to the surface. The arrangement of this logical diagram determines how the triangles will be pushed about and thus the approximate density of triangles in any region. However, it is difficult to predict how much the triangles will be bent, and if the distortion is too great the program will fail.

The program also allows for the various permeability of substances. The geometry of the magnet is broken up into several regions, the permeability of each region is defined to be either the same as air or can be given in the form of a B-H table. In addition the current exciting the magnet can be set to any value.

The results from TRIM depend most critically on the density of the mesh of triangles and the B-H table supplied to the program. Fig. 2.2 shows a plot of $1-B/B_o$ versus Y(in.). B_o Is the field in the median plan at the centre of the pole piece, ie. the very centre of the magnet; this corresponds to the point (1,1) on the logical diagram. The Y axis has its origin at B_o and is parallel to the pole face. This is a standard way of describing the flatness of the field. The curve referred to as the 'finer mesh' employed a logical mesh 17 x 31 with a concentration of triangles near the point (1,1), while the curve labelled 'course mesh' employed a 17 x 28 logical mesh without a special concentration of triangles near the centre of the magnet. They of course describe the same magnet. It is interesting to note that a poor distribution gives a pessimistic result.

To decide what result is correct, TRIM is run at least twice using different densities of triangles. If there is disagreement between the results the mesh density is increased. This process is continued until

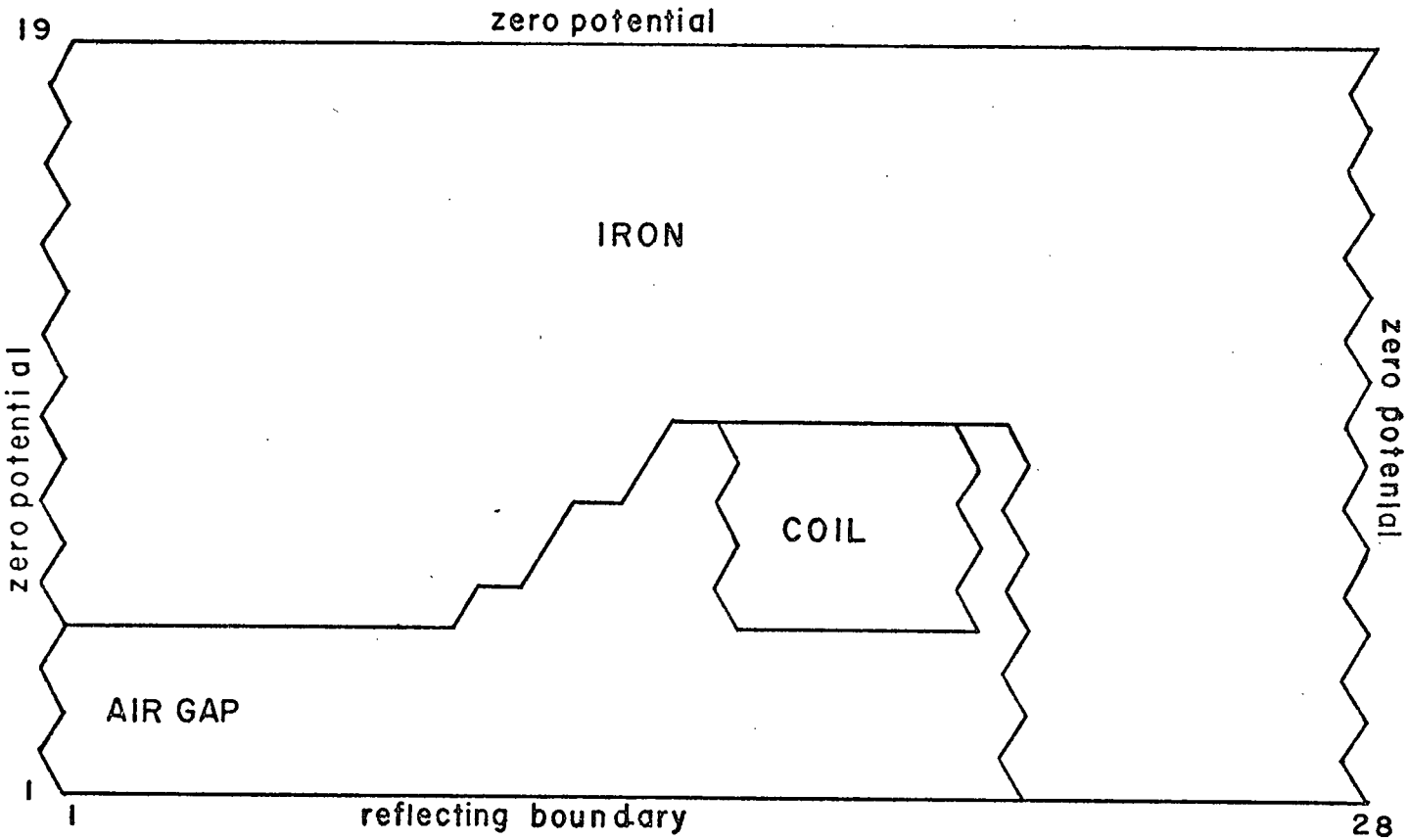

Fig. 2.1. Example of a logical diagram used to map the boundaries for TRIM.

two runs give the same results. Then the solution is mesh independent.

There was concern about the effect of setting the vector potential, equal to zero along the vertical line of symmetry. The program was run with the entire upper half of the magnet, ie. having only a horizontal reflecting line of symmetry. The result is shown in Fig. 2.2 as the curve labelled 'upper half'. It is interesting to note in this case that the maximum field did not occur at the centre of the pole piece, ie. $1-B/B_o$ is not symmetric! The worst variation was only 0.03% and symmetry did re-appear as one got further from the centre, nevertheless this was somewhat disturbing. The cause of the assymetry was thought to be an assymetry in the logical diagram. The ends of the pole pieces could not be represented with exactly the same distribution of triangles, ie. although the geometry is symmetrical the distribution of the triangles, by means of which the relaxation is done, was not symmetrical. This could probably be solved by increasing the total number of triangles so that the program becomes insensitive to such differences. However the results were sufficient to show that the use of a quarter section to map the field did not affect the shape or magnitude of the TRIM predictions.

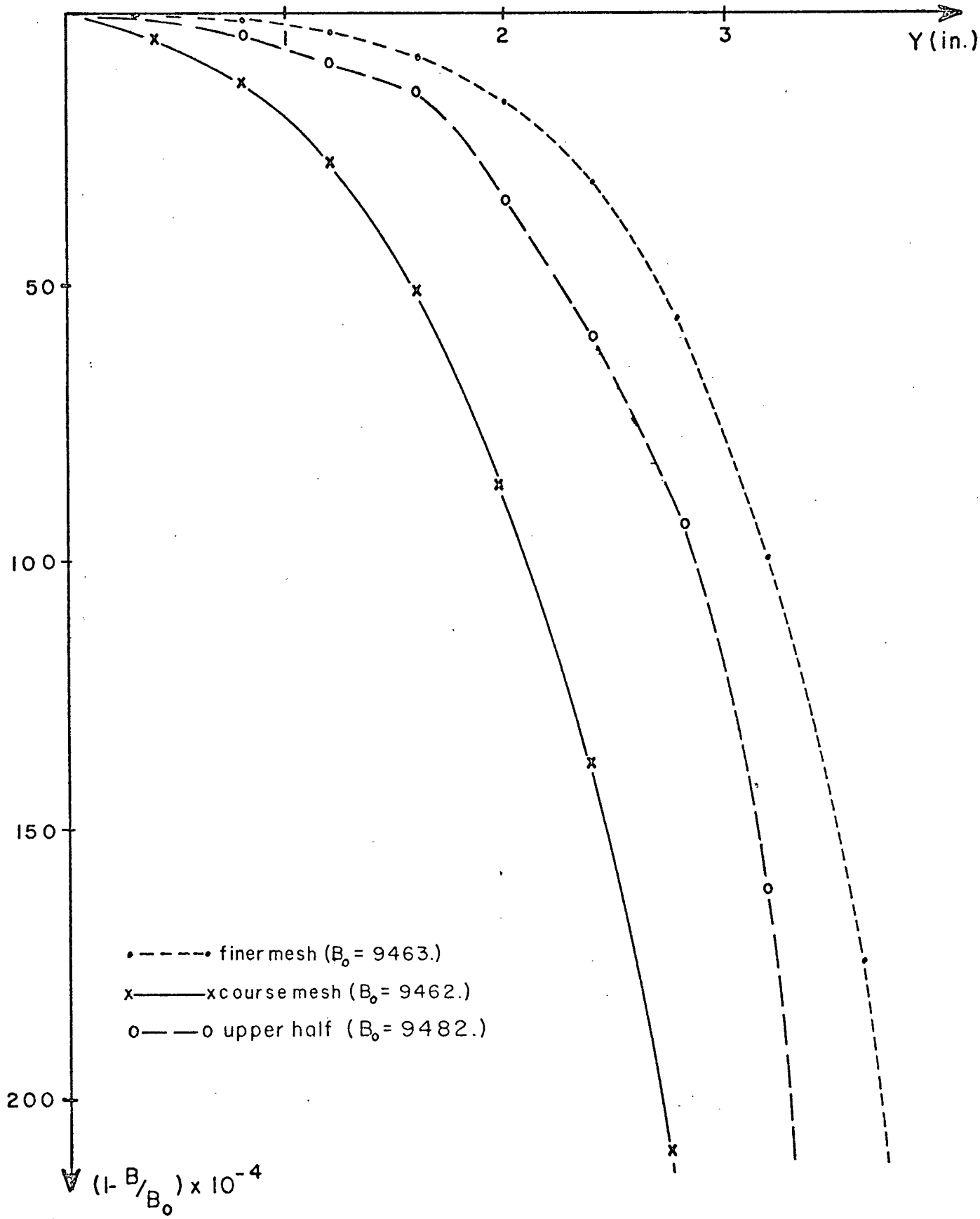

Fig. 2.2. Comparison of the field profile of a magnet due to different mesh densities.

To study the effect of the B-H table on the TRIM output, three comparison runs were made. In the first case 3 points in a straight line were used to describe the B-H curve, the second case used 12 points to describe the B-H curve and the third case used 20 points, see table 2.1, to describe the same permeability for the iron. It was found that the profile, ie. a $1-B/B_o$ versus Y plot, was unchanged but that the maximum field values were; this is shown in table 2.2. This result is really no surprise but emphasizes the need to have the exact permeability for the magnet being designed.

From an inspection of the TRIM output and from a comparison of like results obtained under different operating conditions of TRIM, the field appeared to be smooth and self-consistent to at least 0.05%. This is reasonable for a relaxation program. So the error in the predicted fields is at most 0.05%, and typically .02%.

B-H CURVES

Straight Line		12 Points		20 Points	
B(kg.)	H(oersted)	B(kg.)	H(oersted)	B(kg.)	H(oersted)
0.0	0.0	0.0	0.	0.	0.
20.	20.	11.11	10.	1.1	1.5
30000.	99999.	17.80	100.	2.2	2.1
		19.2	200.	3.0	2.5
		20.0	300.	4.2	3.0
		20.7	400.	6.2	4.
		21.1	500.	7.4	5.
		21.5	700.	8.5	6.
		21.9	1000.	10.0	8.
		30.0	9000.	11.1	10.
		40.	19000.	13.6	20.
		70.	49000.	15.8	40.
				17.27	75.
				17.8	100.
				19.2	200.
				20.	300.
				20.7	400.
				21.1	500.
				21.5	700.
				21.9	1000.

Table 2.1. Permeability functions used in TRIM tests.

B-H TABLE	B_o (gauss)
Straight line	9708.
12 Points	9392.
20 Points	9462.

Table 2.2. Change in the magnitude of field for different B-H tables.

2.2 Calibration Magnet

2.2.1 Determination of the Field

A region of flat field up to 6 kg. is needed for the calibration of probes used in the commissioning of the TRIUMF cyclotron. To provide this a calibration magnet, see Fig. 2.3, was built with an allowance for it to be shimmed, after which it provided a region 4 in. square where B varies by at most 0.2 gauss. To survey this magnet a nuclear magnetic resonance digital gaussmeter by Alpha Scientific Inc. was used with a milling table providing 4" x 8" travel. The NMR was accurate to 10 PPM.

This magnet also provided a test of the program TRIM. Fig. 2.4 shows the field profile from TRIM, and as measured. These curves were taken with a maximum field of 6 kg. Considering the quality of the calibration magnet the results are in agreement. Fig. 2.5 shows the results of the survey of the calibration magnet.

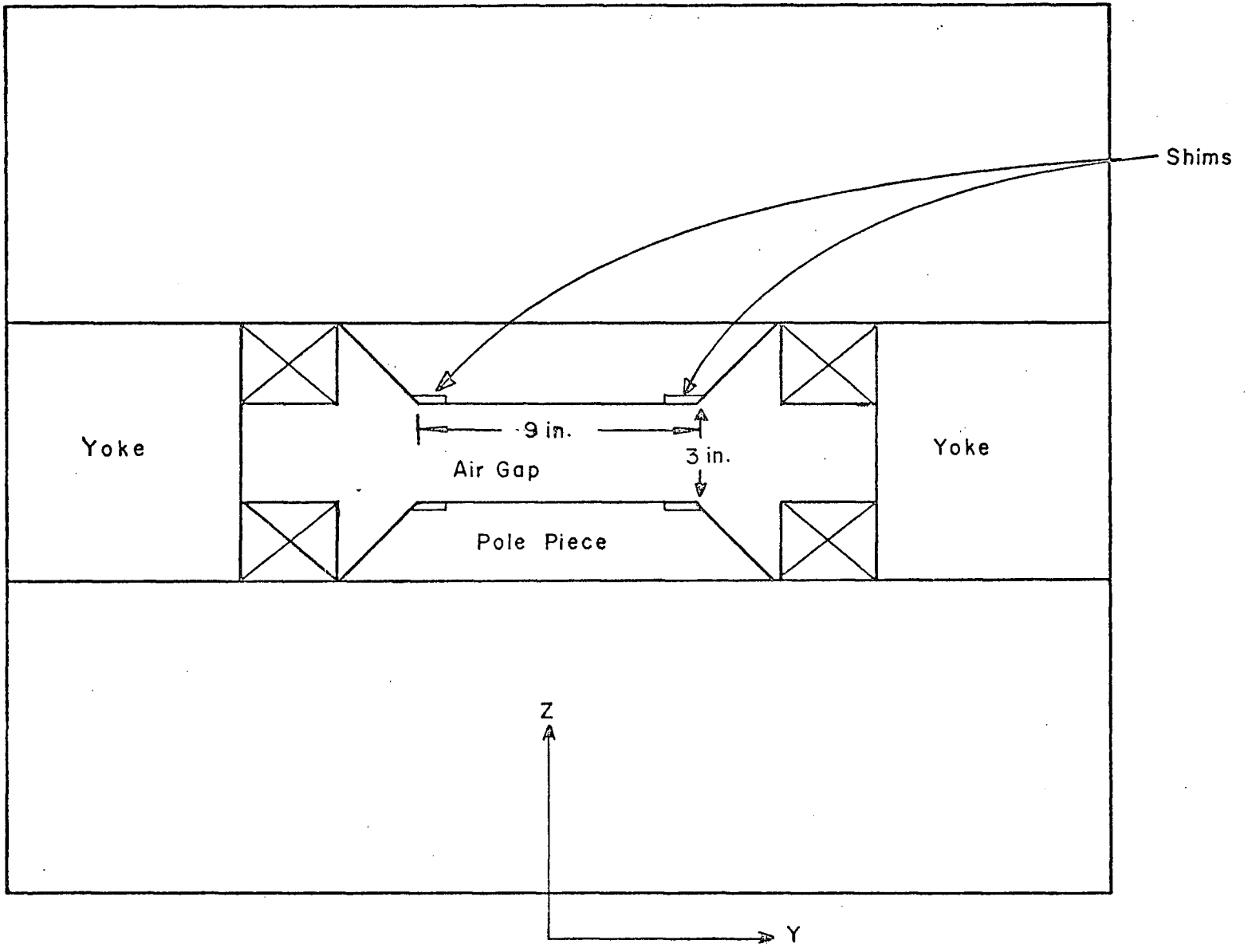

Fig. 2.3. Front view of the calibration magnet.

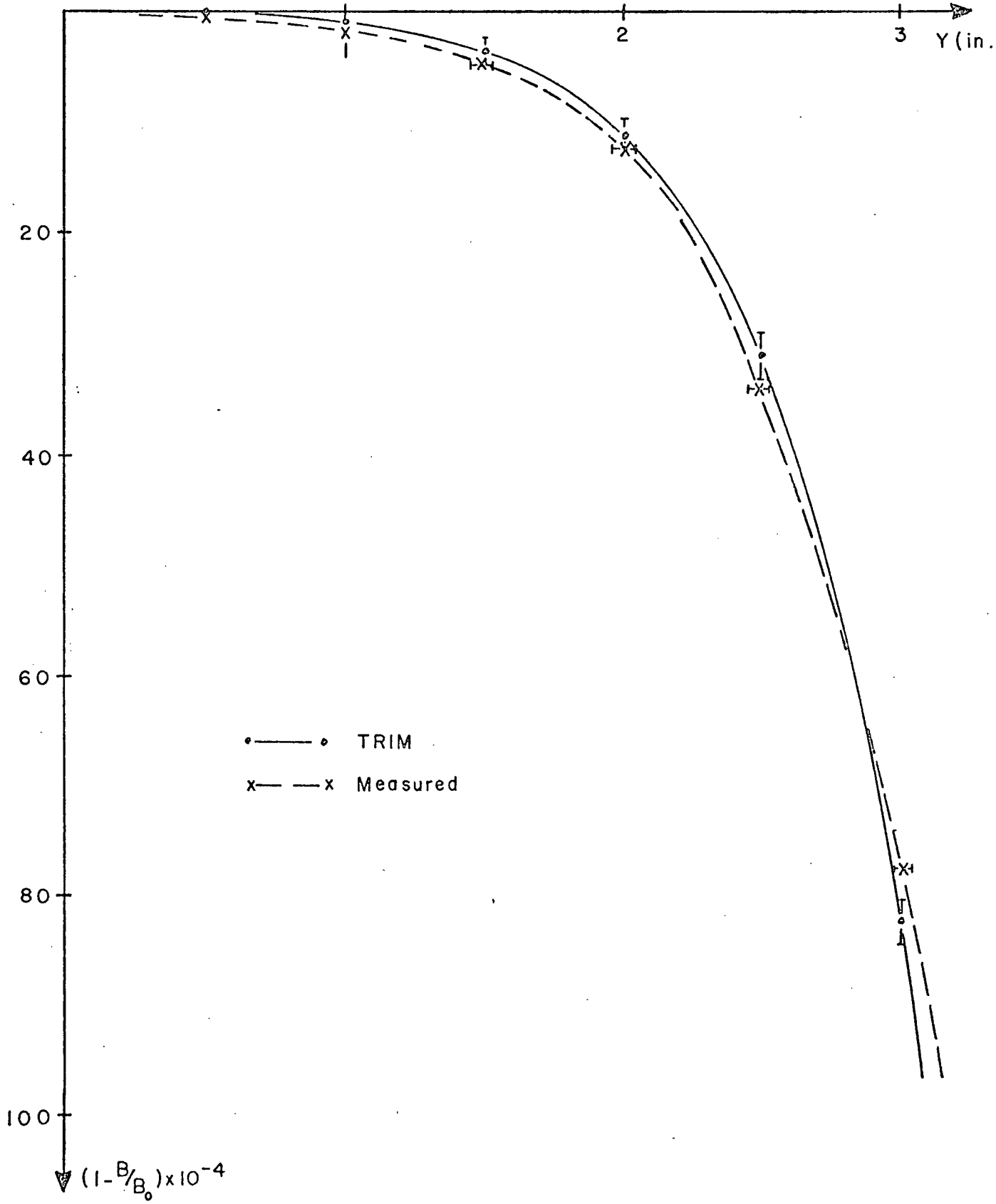

Fig. 2.4. Comparison of the field profile from model measurements and from TRIM.

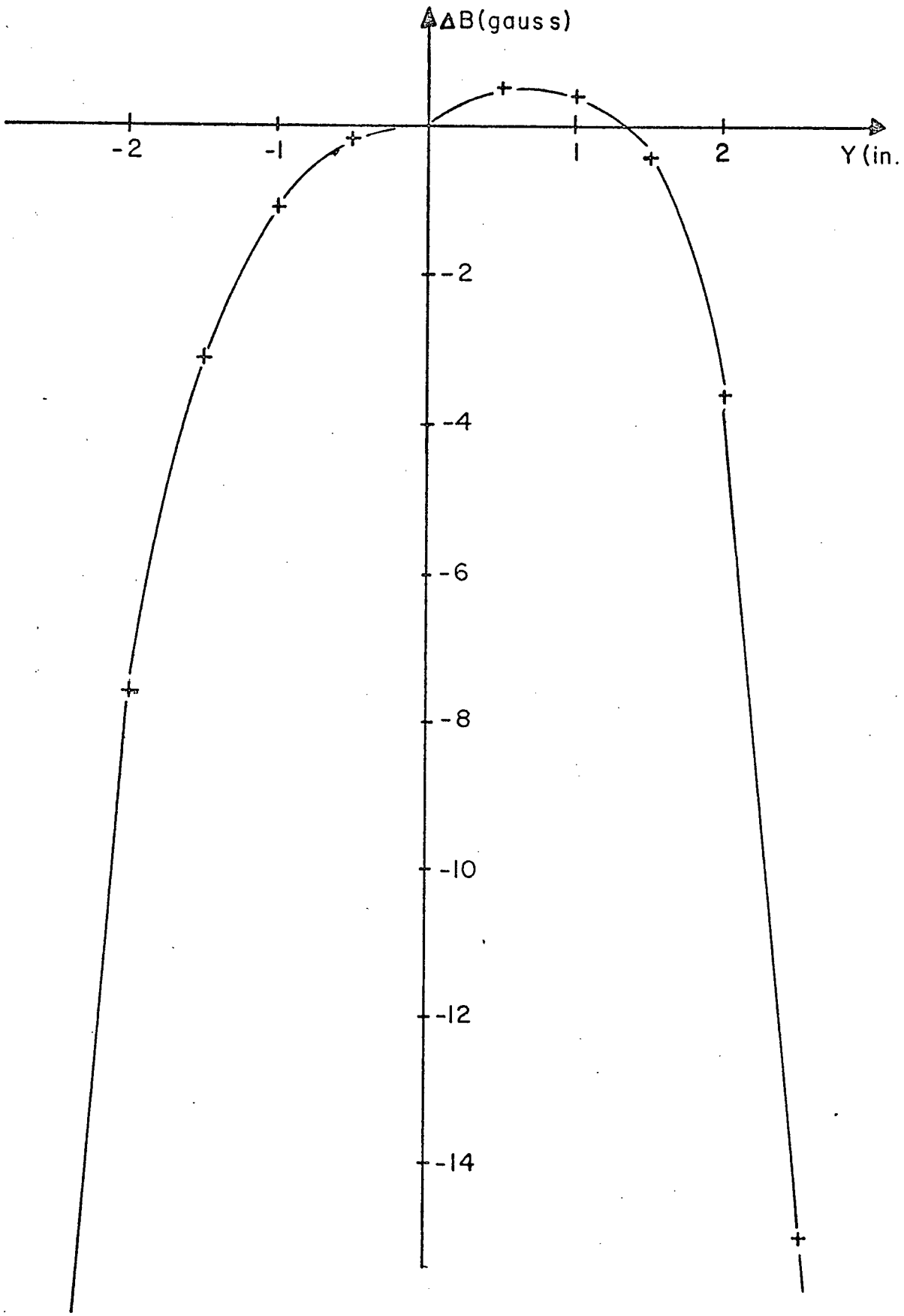

Fig. 2.5. Field variation about the centre of the calibration magnet with B_o=6219.1 gauss.

An area survey revealed a difference of about 1 gauss between the maximum field and the field in the geometric centre of the magnet. This assymetry is a manufacturing fault and accounts for some of the differences in the profiles of fig. 2.4.

A shim 0.035 in. thick was placed on each side of the pole piece. Fig. 2.6 shows a comparison of the TRIM prediction and the measured effect, again very close. The effect of an even thinner shim could be seen by TRIM, but because of the assymetry in the real field a comparison was not possible.

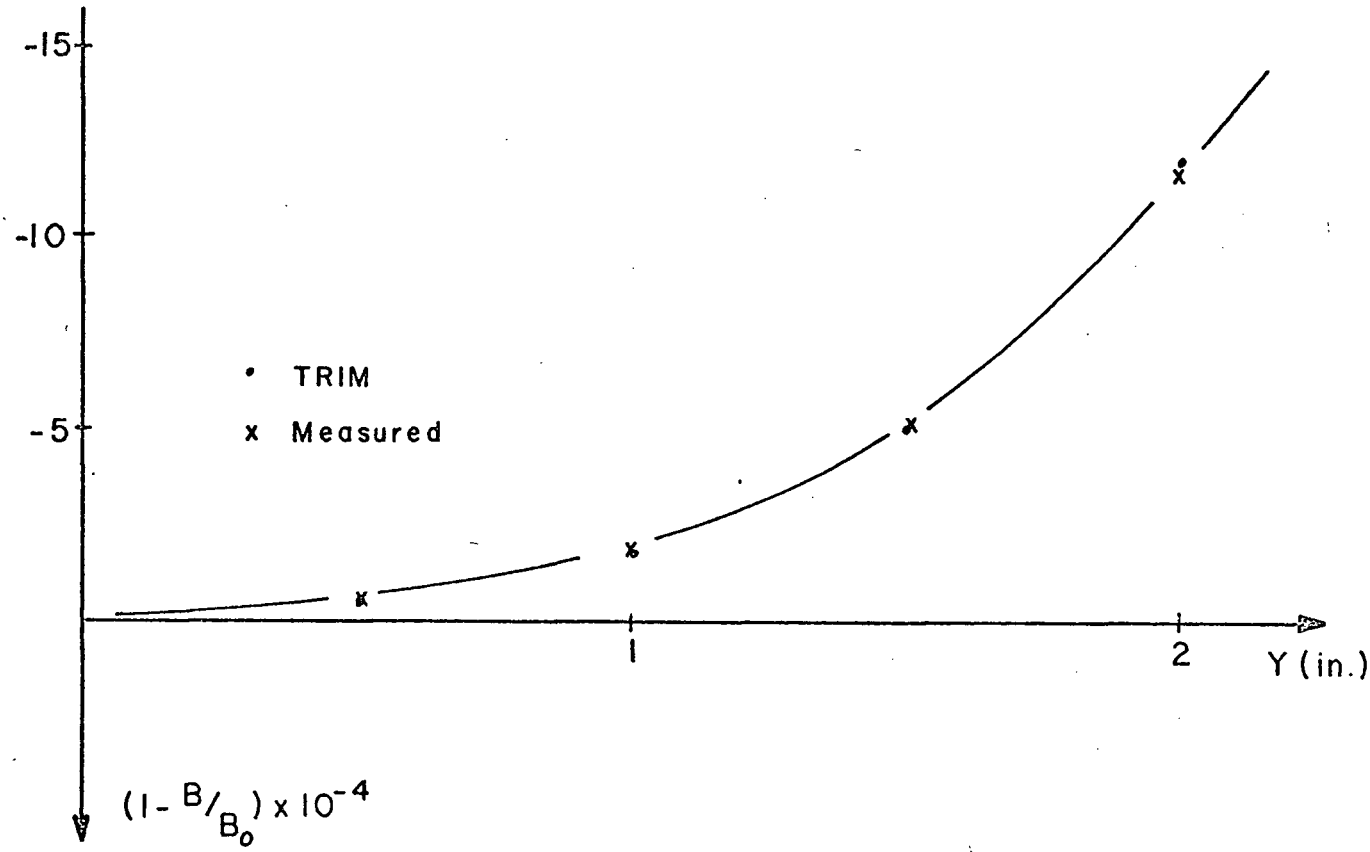

Fig. 2.6. Field profile with 0.035 in. shims in the calibration magnet.

Fig. 2.7 gives the excitation curve of the magnet as measured and as predicted by TRIM. The difference between the results is quite good considering the possible variability of the permeability of the steel. Table 2.3 shows the results of 2 measurements of the permeability of the same grade of steel. For field below 10 kg. they differ from 1200 to 1520 gauss/oersted in permeability.

2.2.2 Analysis of Tolerances

To make a quantitative comparison of TRIM against the magnet measurements we need to look at the tolerances for each method. Letting

$$f = 1 - \frac{B}{B_o} \qquad (2.1)$$

we see that

$$df = - \frac{dB}{B_o}. \qquad (2.2)$$

Since the results of TRIM are good to about 0.02%, then for TRIM

$$df = - \frac{B}{B_o} \times (2. \times 10^{-4}) \qquad (2.3)$$

This produces the error bars shown in Fig. 2.4.

For the magnet survey the NMR has no significant errors, and since it is mounted on a milling table its relative positioning should be within 0.001 in.. However there may be an absolute positioning error of up to 0.050 in..

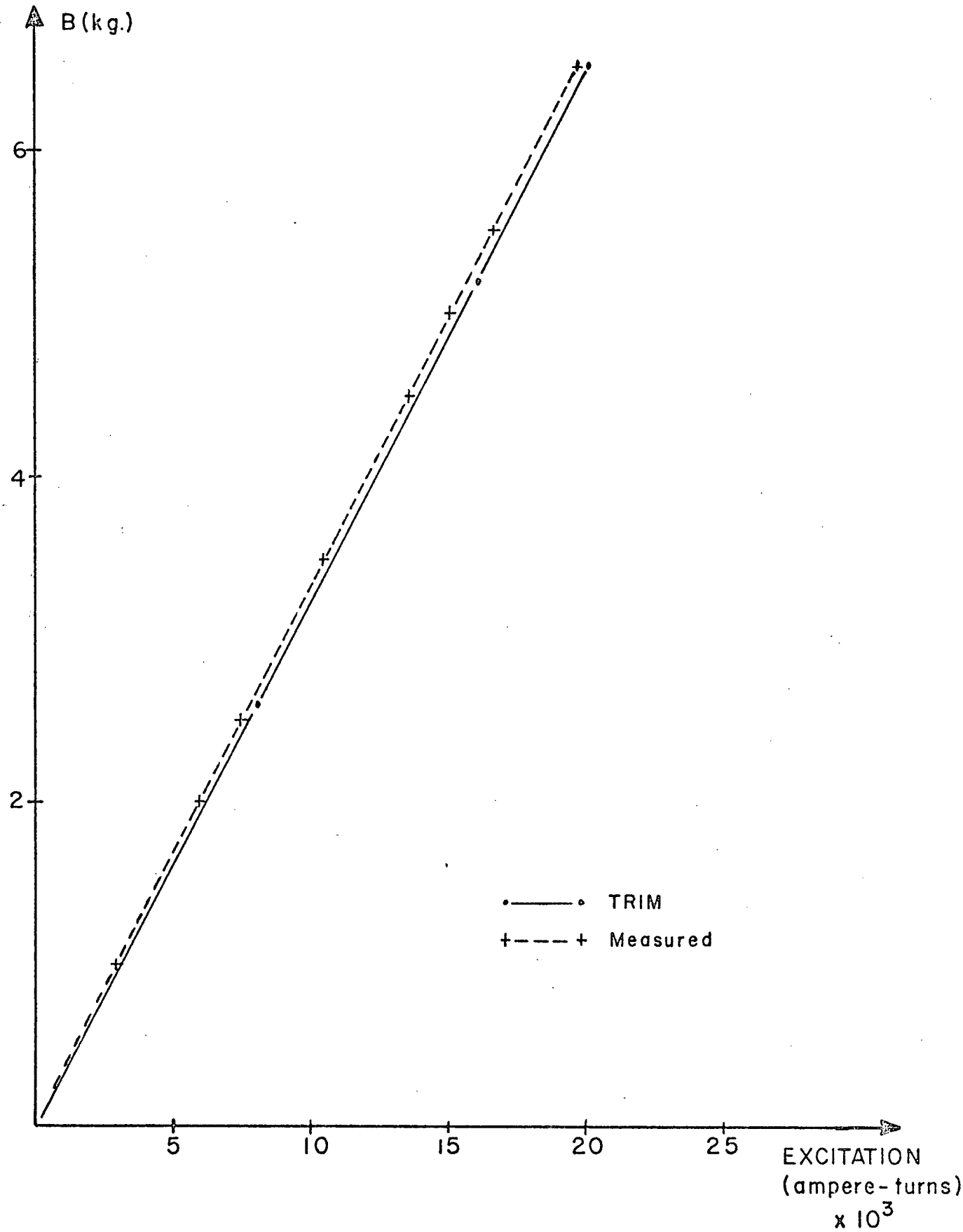

Fig. 2.7. Field in the centre of the calibration magnet as a function of excitation.

H(oersted)	B(kg.)	
	Sample 1	Sample 2
0.		
1.5	1.1	1.3
2.1	2.2	2.9
2.5	3.0	3.8
3.0	4.2	4.8
4.0	6.2	6.7
5.0	7.4	7.9
6.0	8.5	9.2
8.0	10.0	10.3
10.0	11.1	11.4
20.0	13.6	13.8
30.0	15.4	15.3
40.0	15.8	15.8

Table 2.3. Permeability for 2 samples of 1010 steel, as measured by the U.B.C. engineering department.

This is represented by the error bars in Fig. 2.4. There is also the restriction that the magnet can only be machined to within 0.1%. Thus we are justified only in looking for agreement within this percentage.

Looking at Fig. 2.4 it is clear that the profiles agree within the error limits.

2.3 The Combination Magnet

2.3.1 Trim

The extraction orbits for particles of energies from 150 to 500 Mev. were determined. How this was done will be discussed in the next chapter. Using this information a magnitude of field and area of field is defined such that any beam extracted from the cyclotron can be diverted into a fixed beam line. It is the combination magnet that provides this field.

The program TRIM was now used to study the characteristics of the combination magnet. This is an H magnet with a variable width pole which is used to bend the beam of protons as they emerge from the cyclotron.

The proposed combination magnet design was studied with the aid of TRIM and, based on the results, the design of the combination magnet was fixed. Fig. 2.8 is a photograph of the 1/10 scale model. Fig. 2.9 shows the lower half of just the iron component of the magnet.

Fig. 2.8. 1/10 Scale model of the combination magnet.

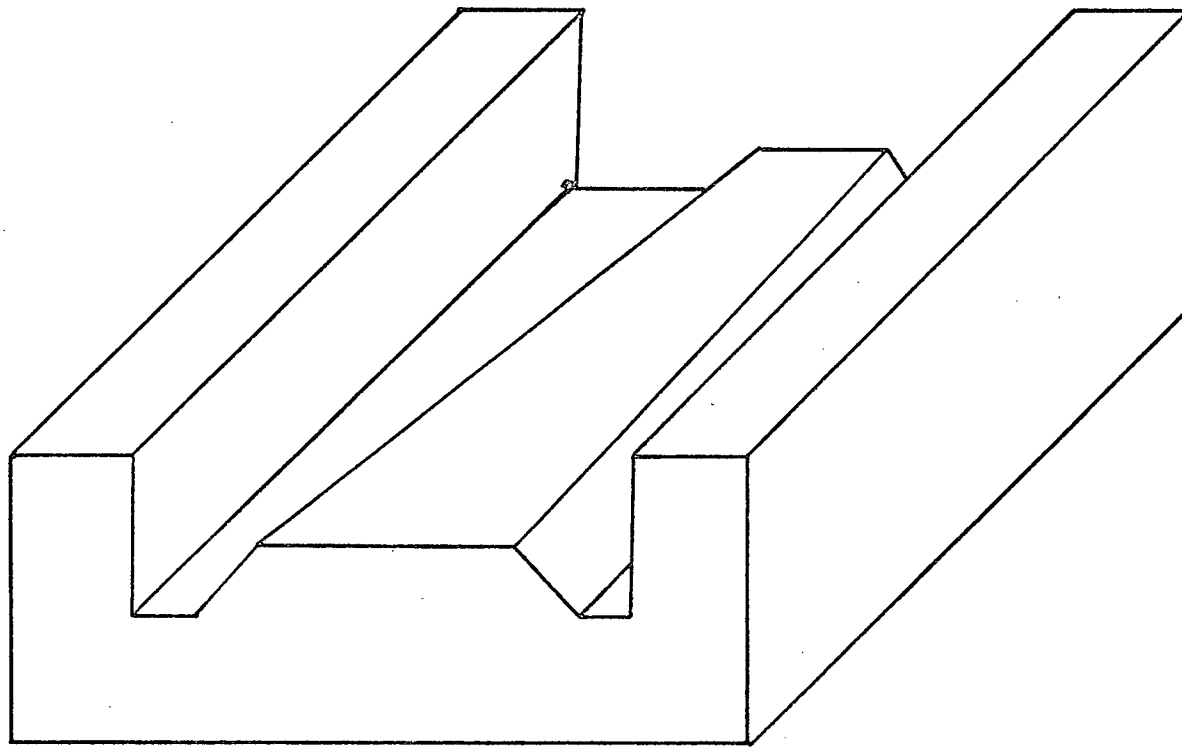

Fig. 2.9. Iron component of the lower half of the combination magnet.

The important feature is that the pole is 24 in. wide at the end where the beam enters and 10 in. wide where the beam exits.

What was required of TRIM was an appreciation of the effect of varying pole widths, and the effect of different excitations. The design requirements call for less than a 0.01% variation in the field in the region where the beam travels.

Fig. 2.10 shows the profile of the field for the entrance end, centre and exit end. At the entrance the field increases beyond the accepted range. However since TRIM assumes an infinitely long magnet it is uncertain what the true profile will be at the exit and entrance ends. It is thought that, if necessary, any significant effect can be corrected by shims.

Fig. 2.11 shows the profile of the field for various excitations. These are for the mean pole width of 18 in. The field shape is not very sensitive to current changes and flattens out with decreased excitation.

2.3.2 Comparison With 1/10 Scale Model

The 1/10 scale model of the combination magnet was powered and measurements made on it. The probe used to measure in the small gap (0.4 in.) was FH 301 Siemans hall plate mounted inside a ¼ in. thick bar of plexiglass.

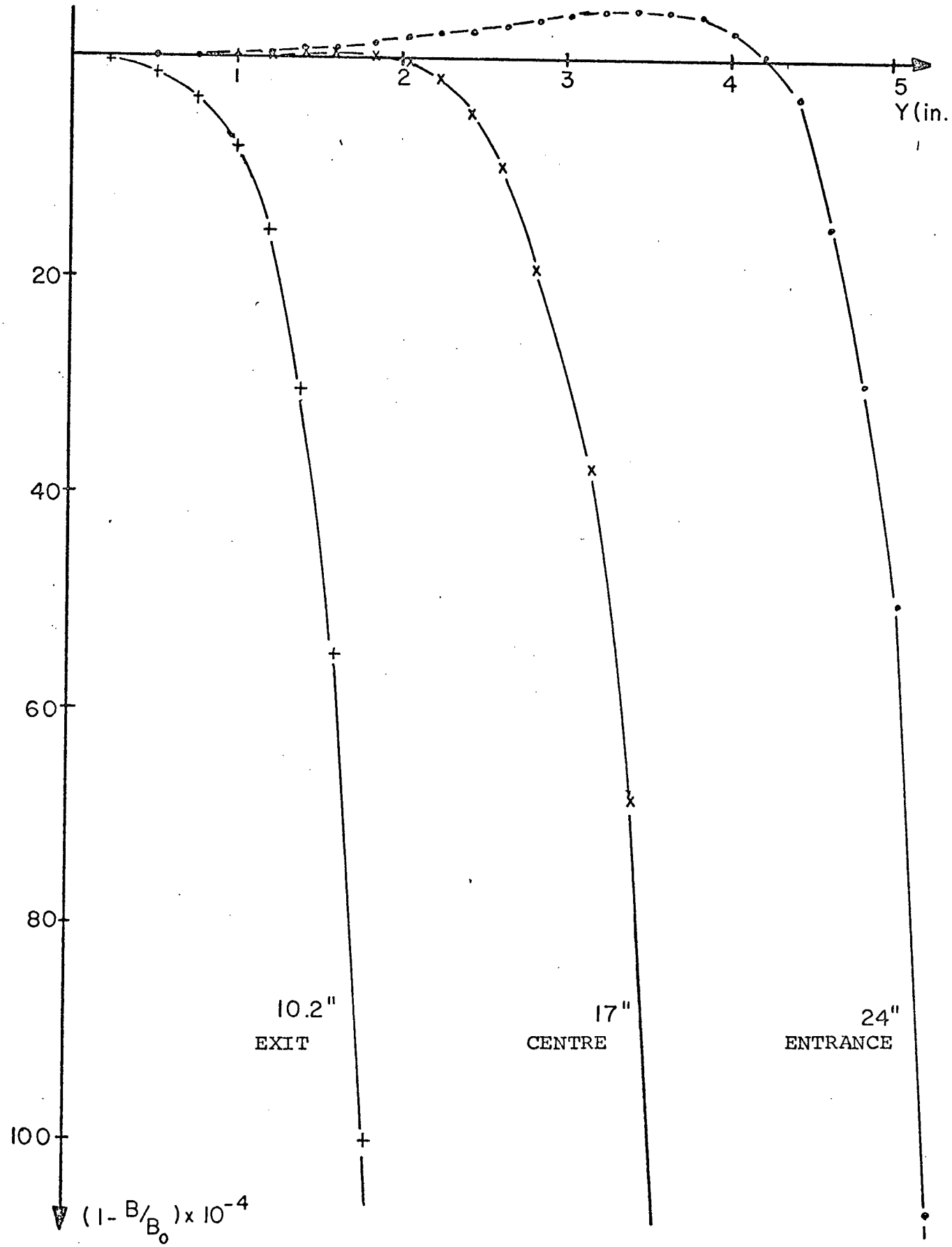

Fig. 2.10. Field profile as a function of the pole width; excitation is 40,000 ampere-turns.

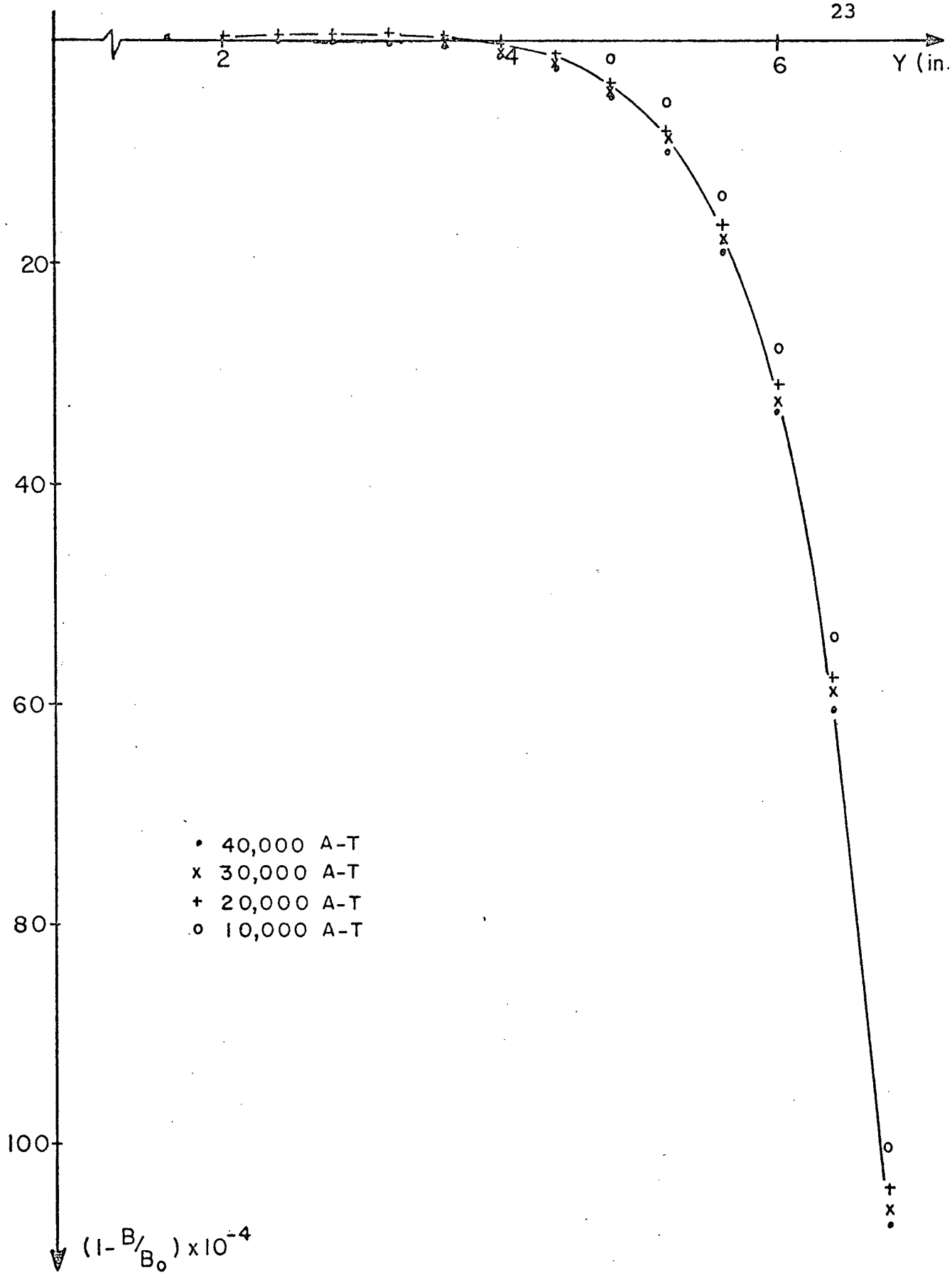

Fig. 2.11. Field profile as a function of excitation, as predicted by TRIM.

It was not temperature compensated in any way. The size of this probe was restricted by the small space between the poles of the scale combination magnet into which it had to fit. The dimensions of the pole piece of the combination magnet were changed slightly before the model was built and so the model differs from those used for the TRIM runs. The widths of the pole piece are, in full scale, 24 in. at the entrance end, 12 in. at the exit end, and 18 in. at the centre.

Fig. 2.12 shows the profile for the pole of width 18 in. at several excitations as measured on the 1/10 scale model. Comparing with Fig. 2.11 we can see the ½ in. displacement of the two data sets. The FH 301 Hall probe has a temperature coefficient of -0.15% per ^{o}C. Supposing a 1 ^{o}C variation in the temperature this will cause an error in the measured B's such that

$$df = \pm 15 \times 10^{-4}. \qquad (2.3)$$

Comparing Fig. 2.11 and Fig. 2.12 we see that they agree well within these uncertainties.

Fig. 2.13 shows a comparison of the excitation curve as predicted by TRIM and as measured using two different power supplies. The measurements were first done with a Hewlett Packard 6543A power supply; but since this was only stable to 1% the measurements were repeated with large current supply built by Alpha Scientific. The currents were determined simply from meter readings. There is also a possibility, as with

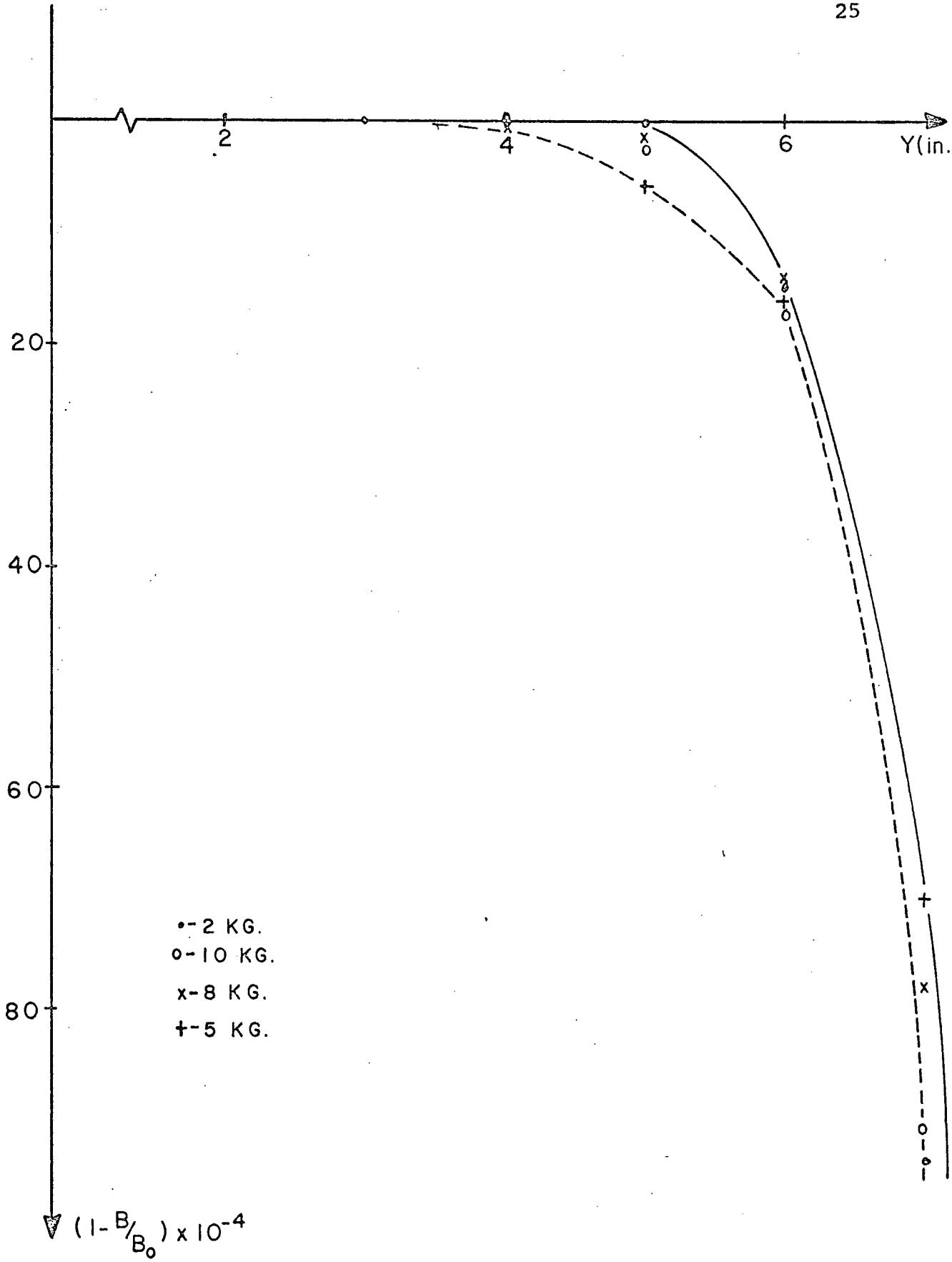

Fig. 2.12. Field profile of the combination magnet from model measurements as a function of B_o.

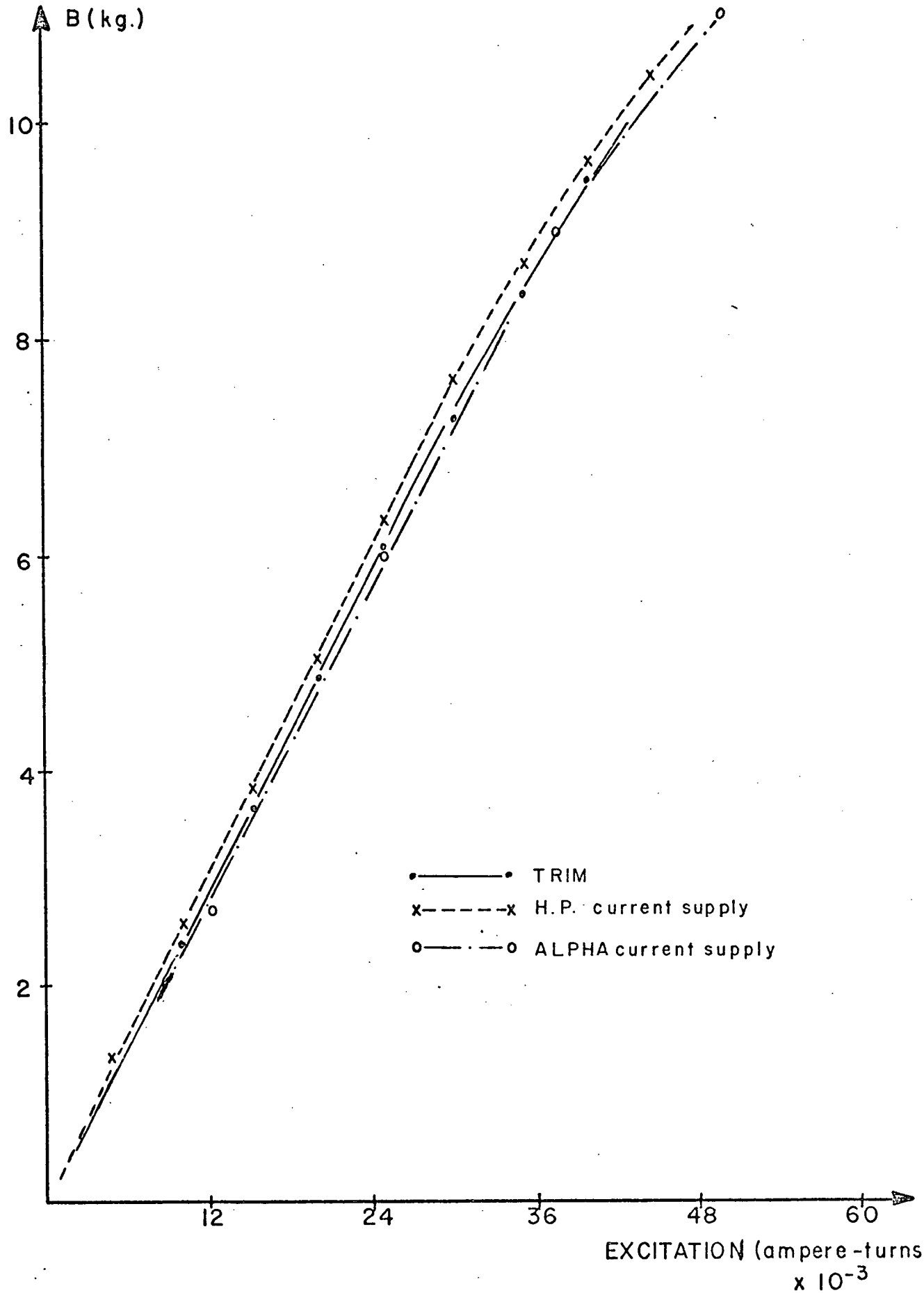

Fig. 2.13. Comparison of the excitation of the combination magnet between the model measurements and TRIM.

the calibration magnet that the permeability for the model was different than that used by TRIM. Considering these uncertainties, the differences between TRIM and the measurements are not significant.

2.4 Conclusions

TRIM seemed to work satisfactorily in its ability to predict the calibration magnet field. Because it and the model measurements gave the same results for the combination magnet they have equal ability to predict the full scale magnet field. However, since the model is 3 dimensional and the program only 2 dimensional, more information can be obtained from the model.

TRIM was tedious to run and required a large amount of computer time, about 200 min. of cpu time on the U.B.C. 360/67 were used to make the combination magnet studies. However the model, because of its size, requires tight tolerances in construction and measurement to produce comparable accuracy. The great advantage of TRIM is the ease with which changes in magnet design can be made.

3. EXTRACTION REGION SURVEY

3.1 Introduction

The commissioning of the TRIUMF cyclotron requires a measurement of the field between the return yokes through which the beam will pass when extracted from the machine. This survey must be sufficient to enable us to determine the trajectory of a beam having any energy desired, and thus determine the locus of the stripping foil and the cross-over point of the extracted beams. The energy of the beam may be changed by changing the radial position of the stripping foil. If at the same time the azimuthal position of the foil is suitably varied, the orbits of the extracted beams may be made to pass through a common point located outside the cyclotron. This cross-over point defines the location of the combination magnet. The variance of the trajectories dictates the size of the pole piece of the combination magnet, as mentioned in chapter 2. It was initially planned to be able to extract two beams simultaneously each capable of energies from 150 to 520 Mev.

It is also important to determine the optical properties of the beam. The fringe field of the cyclotron is dispersive while the combination magnet provides some focusing. In all, the system is dispersive and the remaining beam transport elements must correct this.

To decide on the feasibility of such an extraction system, measurements were done on a 1/20 scale model of the cyclotron magnet using a 1/20 scale model of the combination magnet. From this work it was determined which of the two possible directions of rotation for the beam would be most satisfactory and some of the implications of the technique.

When a 1/10 scale model of the cyclotron had been built it was decided to repeat the measurements of the extraction region field. In the 1/20 model measurements of the magnetic field significant areas just inside the yokes were missed and values had to be extrapolated for the analysis. These areas could now be measured on the 1/10 scale model. The locus of the stripping had to be known precisely enough that the necessary maneuverability of the stripping foil mechanism could be decided upon and incorporated in its construction. To give us the better knowledge needed it was decided to conduct a series of measurements using the existing model. An assessment of the interaction of the combination magnet and the cyclotron magnet was also desired. For this our 1/10 scale model of the combination magnet could be used with the cyclotron model. In addition, a new set of model measurements would give us a chance to gain some experience in extraction region survey work to prepare us for the full scale studies. A knowledge of what the field looks like allows us to design our full scale

measuring apparatus more effectively, and the exercise in analysis gives us practise in running the software needed for the beam diagnostics, as well as an opportunity to update our computer programs.

Therefore it was decided to investigate the change in locus of the stripping foil for different extractions regions, different excitations of the cyclotron magnet, and differences due to the combination magnet.

3.2 Survey Techniques

The irregular geometry of the extraction region makes it difficult to automate this survey. Since the analysis process only demands a 20 gauss tolerance in the measurements, it was thought that a manual survey would suffice. For this, a 1/8 in. aluminum plate was cut to a shape that matched the contour of the yokes so that it could be placed in this region. Several aluminum brackets were constructed to support this plate parallel to the pole pieces, and at a height such that the hall plate used would be on the geometric median plane.

It was decided to use a polar co-ordinate system with the cyclotron centre as the centre of this system. Data that extended well into the internal field was needed, but the data that was to be collected in the extraction area was more important. And since the internal surveys were made with 1^{o} increments and at .5 in. intervals

this grid would suffice for the data of the extraction survey that overlaps the internal survey. However the grid was decreased to $\frac{1}{2}^{o}$ and .25 in. increments in the region beyond the 32.0 in. radius, ie. in the space between the yokes and out to where the combination magnet would be.

A series of holes on arcs 2 in. apart were drilled in the metal plate to provide the angular positioning, and the probe indexing mount was built to allow it to move radially between the arcs to provide the radius settings. Fig. 3.1 shows a computer plot of the array of pin holes to be drilled in the plate. The first radius is at 21.6 in.; the large gap is 8 in. and is the narrowest space between two neighbouring yokes. It is apparent in the figure which radii have $\frac{1}{2}^{o}$ increments and which have 1^{o} increments.

To construct the template, it was laid in position, a radial line was scratched on its surface and a point of known radius marked on this line. Using this as the origin of a rectangular co-ordinate system a computer was used to calculate the (x,y) co-ordinates of the points in the first figure. These values were used as the settings of the table of a milling machine that was employed for the drilling.

The Hall probe used for the measurements was mounted on aluminum supporting pods that in turn were sitting upon a flat plexiglass plate that formed the base

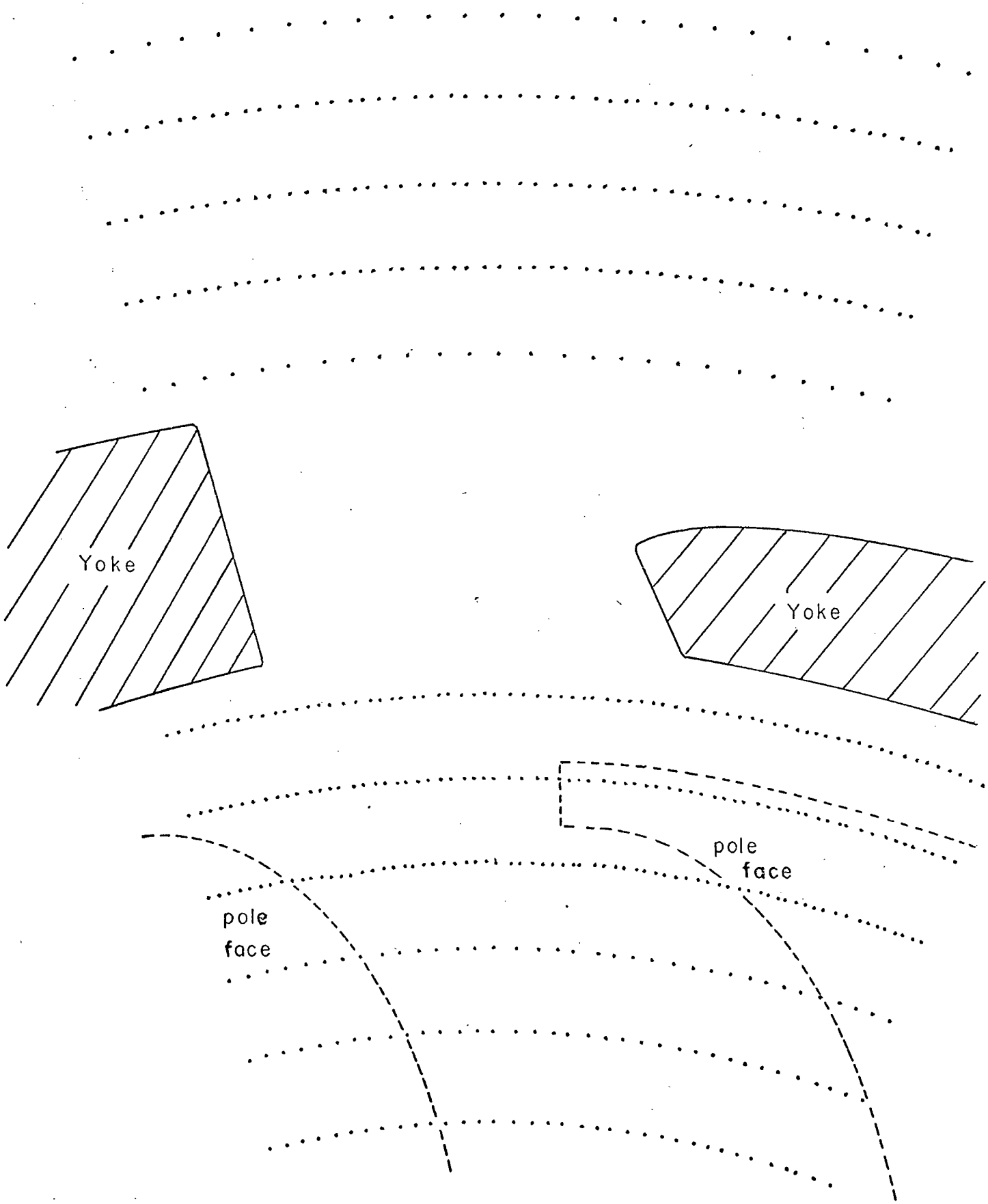

Fig. 3.1. Positions of the pin holes for the machining of the template.

of the probe. 17 Pins, space ¼ in. apart, were mounted in line down the centre of this base plate. The pins could be in either the 'up' position so that they would not extend beneath the base or in the 'down' position so that they did protrude under the base. These pins fitted into the holes in the aluminum plate. Using 2 pins, 2 in. apart, the probe could be advanced or retarded radially in at least ¼ in. steps. Thus the aluminum acted as a template for this adjustable probe.

A Siemans FH 301 Hall plate was chosen for this work because of its small size. It is about 0.14 in. square and less than 0.02 in. thick. It was mounted ½ in. from the end of a ¼ in. thick plexiglass bar. A cap was cut in the plexiglass at the end so that the hall plate could be held inside the probe, ie. having 1/8 in. of plexiglass above and below it. The bar was 15 in. long and supported at one end, above the base plate, by the afore-mentioned aluminum pods. For most of the work the Hall plate was positioned 4 in. beyond the centre of the pin nearest to it. But for measurements with the combination magnet model it was extended to 8 in. beyond the nearest pin. For data at radii less than 35.0 in. the probe was inside the magnet and pointed outward, and for the data at larger radii the probe was outside the magnet, pointing inwards. This tightens the tolerances on the radial position of the arm but also

makes the positioning of the probe easier, as will be seen.

The Hall probe used in this survey had to fit between the coils of the 1/10 scale combination magnet, a space of about 0.3 in., so the size of the Hall probe had to be kept small. But it is very difficult to temperature stabilize the Hall plate with such a size probe. Consequently the Hall probe was not temperature compensated at all. The FH 301 has a temperature sensitivity of -0.15% per ^{o}C according to the Siemans company. Thus a $1^{o}C$ variation causes an 18 gauss error in a 6 kg. field or a 13 gauss error in the more usual 4 kg. field.

The template was levelled to 0.1^{o} each time it was installed. Measurements were made to check the angular alignment of the Hall plate with respect to the base of the probe, and the Hall plate was adjusted until the tilt in any direction was less than 0.6^{o}. A combined misalignment with the Hall probe sitting on the template cause at most a 4 gauss error due to the Hall plate detecting a horizontal component of the field.

After the template was machined the relative positioning of the pin holes were checked and found to be at worst, in error by ±0.008 in., but usually were within 0.004 in. The radial position of the Hall probe centre with respect to the pins was checked using the fringe field of the cyclotron. This can be done by comparing the readings

when the probe is inside the magnet, pointing outwards, and the Hall plate is sitting on the 35.6 in. radius: and when the Hall plate is on the same radius, but the probe mount is outside the magnet pointing inward. At this radius the gradient in the model is about 1 kg. per in. This check could be done in a few seconds and was repeated quickly for the same azimuthal position and for several other azimuthal positions until confidence was achieved that the probe was on the correct radius within 0.001 in. In the largest gradients measured, those near the yokes and underneath the coils, the total positioning error could cause an error in the measurements of up to 30 gauss. However a 10 gauss error would be typical.

Now considering together the positioning, alignment, and calibration errors together, see table 3.1, a rms sum of the worst cases imply a 35 gauss error; but a typical result would have a 17 gauss uncertainty.

Quantity	Variance	Field Errors (gauss)	
		Maximum	Minimum
Temperature	1^{o}	18	13
Angular alignment	0.6^{o}	4	4
Position	0.009	30	10
RMS. Sum		35	17

Table 3.1. Summary of measurement errors.

It may be said the greatest errors will occur in the region of most importance, ie. under the coil. However the area of such very large gradients isn't great and there is a high density of data points here. It should be noted that because this survey was manually performed there are a few data points wildly in error due to the operators fatigue. The analysis was not sensitive to such mistakes.

The experience from the 1/20 scale model measurements indicated that a tolerance of + 20 gauss was acceptable. So this system was approved and the survey work initiated.

3.3 Analysis Techniques

To track the trajectory of the beam, the position and momentum of the beam as it strikes the stripping foil and the field that the particle travells through, after passing through the stripping foil, must be known. The momentum and position of the beam are produced by a routine called CYCLOPS which uses the data of an internal field survey.[7] The data accumulated using the template must be normalized to fit the internal data used by CYCLOPS. Thus for each extraction survey there must be a corresponding internal survey.

This normalization is provided by a program called BCONV.[8] It uses the data from the external survey and

that part of the extraction region survey that overlaps this data and determines the normalization of the extraction data required. In addition BCONV also checks: the alignment of the extraction survey co-ordinate system, giving us the concentricity of the two coordinate systems, what the first angle of the extraction region data is with respect to the internal survey data, and finally what the relative twist of the second system is. If necessary these quantities can be used to correct the extraction survey data.

A program called BFIELD[9] fourier analyzes the normalized extraction field data. The coefficients are data for a ray tracing program called STRIP[10] that, together with the information from CYCLOPS, determines the trajectories of the particles. The position of the cross-over point, as determined by the 1/20 scale model work, is supplied to STRIP. Using this point it traces backwards to determine what position the stripping foil had to be in for the beam to pass through this point. Thus the locus of the stripping foil was determined.

3.4 Survey Description

First an internal survey was done, measuring a 180^{o} section of the model cyclotron magnet. Then an extraction survey was made for two adjacent extraction regions. This will tell us how sensitive the beam trajectories

are to small variations in the field shape and if a separate analysis of the different extraction regions will be required on the full scale magnet.

In the second region surveyed, another survey, both internal and external, was done at a higher current setting, called #2. This is to tell us how the locus of the stripping foil changes with excitation of the cyclotron magnet.

After this, part of the template was cut away so that the model combination magnet could be placed in position. Fig. 3.2 shows the present plan for positioning the combination magnet. The model was at about a 45^{o} angle to a radial line, its radius was positioned to about $\frac{1}{4}$ in. and thin slices of wood used to keep the two magnets apart. A program that aligns the combination magnet field, as independently surveyed, with the extraction field, verified that the combination magnet was in its correct position.

Without the combination magnet being excitated the internal field and external fields were surveyed. Spot checks were made at radii from 25.0 in. to 35.0 in. and in both valley and hill fields to search for any change in the internal field as a function of combination magnet excitation. The averages $\overline{B}(R)$, averaging over 60^{o}, were compared with and without the combination magnet present. In addition the internal field at 30.0 in.

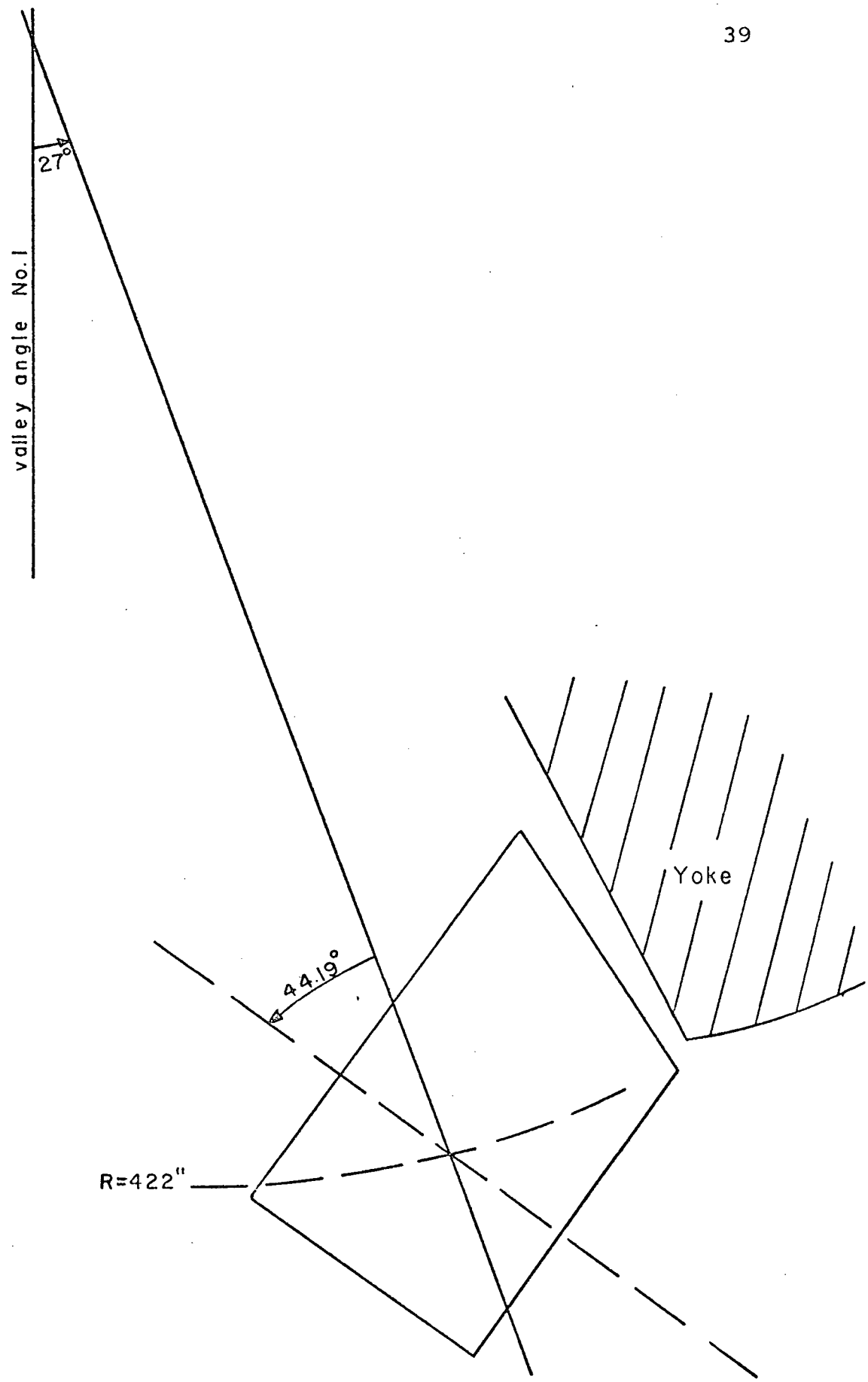

Fig. 3.2. Position of the combination magnet with respect to the cyclotron.

was measured over 180° with no excitation, and then with 43,700 ampere-turns (full scale) excitation, and the results compared.

Finally, extraction field surveys were made with the combination magnet excited to 20,000 ampere-turns and 43,700 ampere-turns. These respectively produce a 5 kg. field needed to bend the 400 Mev. beam and a 10 kg. field to bend the 200 Mev. beam. The cyclotron excitation had not been altered so the normalization constant would not have changed. It should be noted that the only available current supply for the combination magnet was only regulated to 1%.

3.5 Results

Fig. 3.3 shows a contour map, generated on our 360/67, of one of the data sets taken using the template. The contour lines are in hundreds of gauss.

Fig. 3.4 shows a comparison of the stripping foil locus from the 1/20 scale model measurements with the locus from the valley 2, excitation #2 survey. The points in the curves are at 50 Mev. intervals. Fig. 3.5 gives the foil locus for the two extraction regions studied, ie. valley 1 and valley 2; both at the low or #1 excitation. This figure also gives the locus for valley 2 at the higher or #2 excitation. The points plotted start a 200 Mev. and go to 500 Mev. in 50 Mev. intervals.

Fig. 3.3. Contour plot of the magnetic field as measured by a typical extraction region survey.

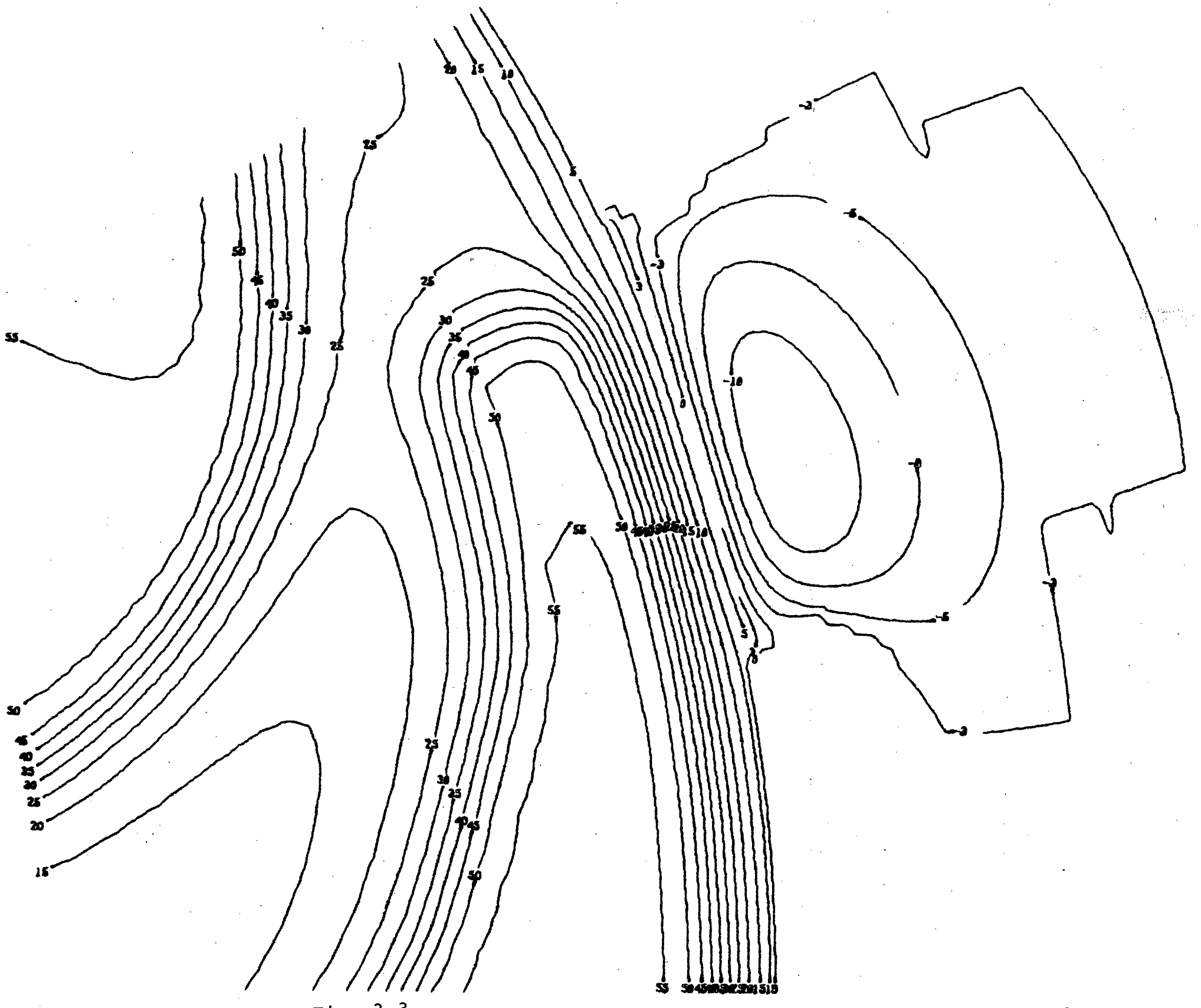

Fig. 3.3

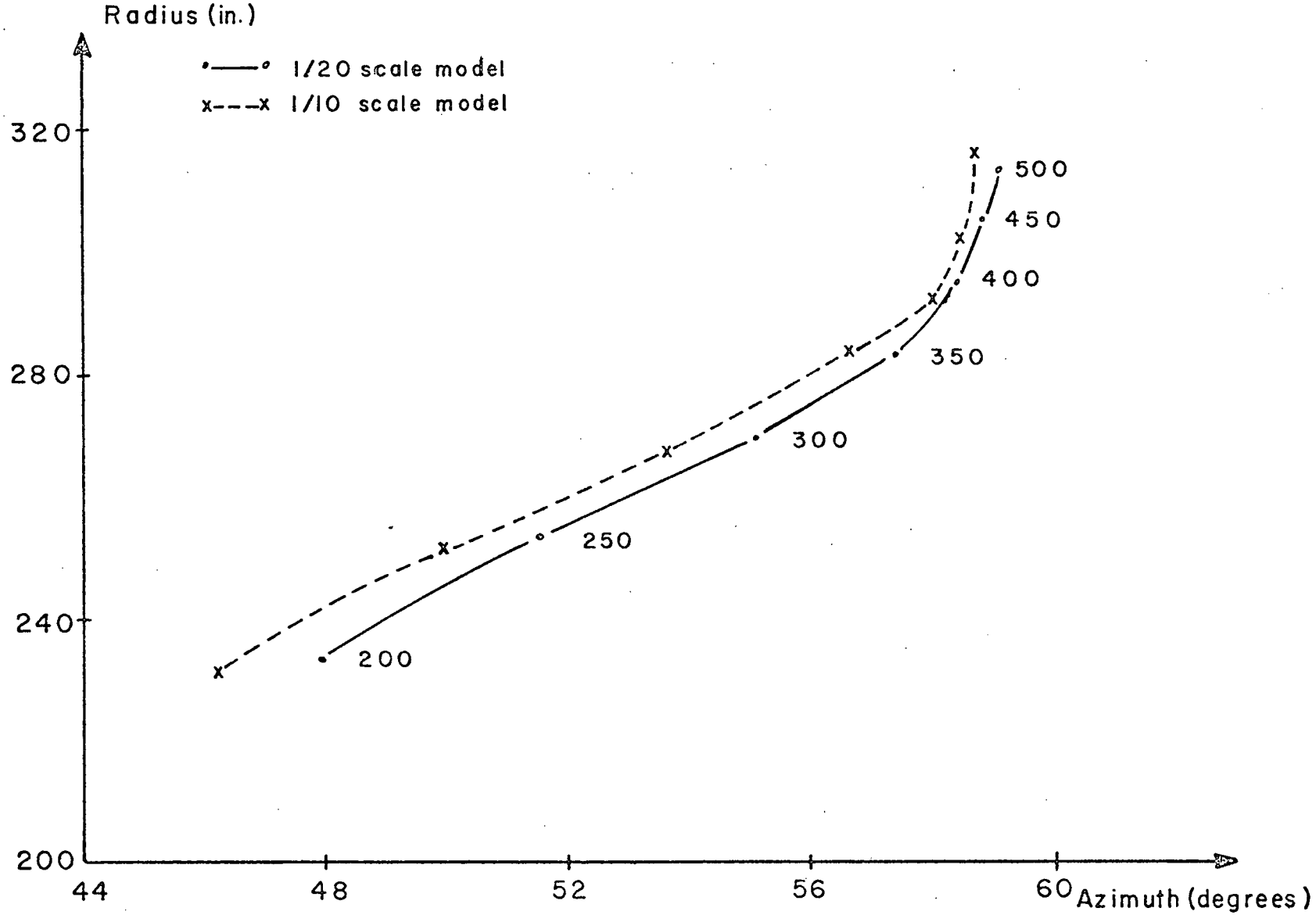

Fig. 3.4. Stripping foil locus from 200 to 500 Mev. from the 1/10 and 1/20 scale model studies.

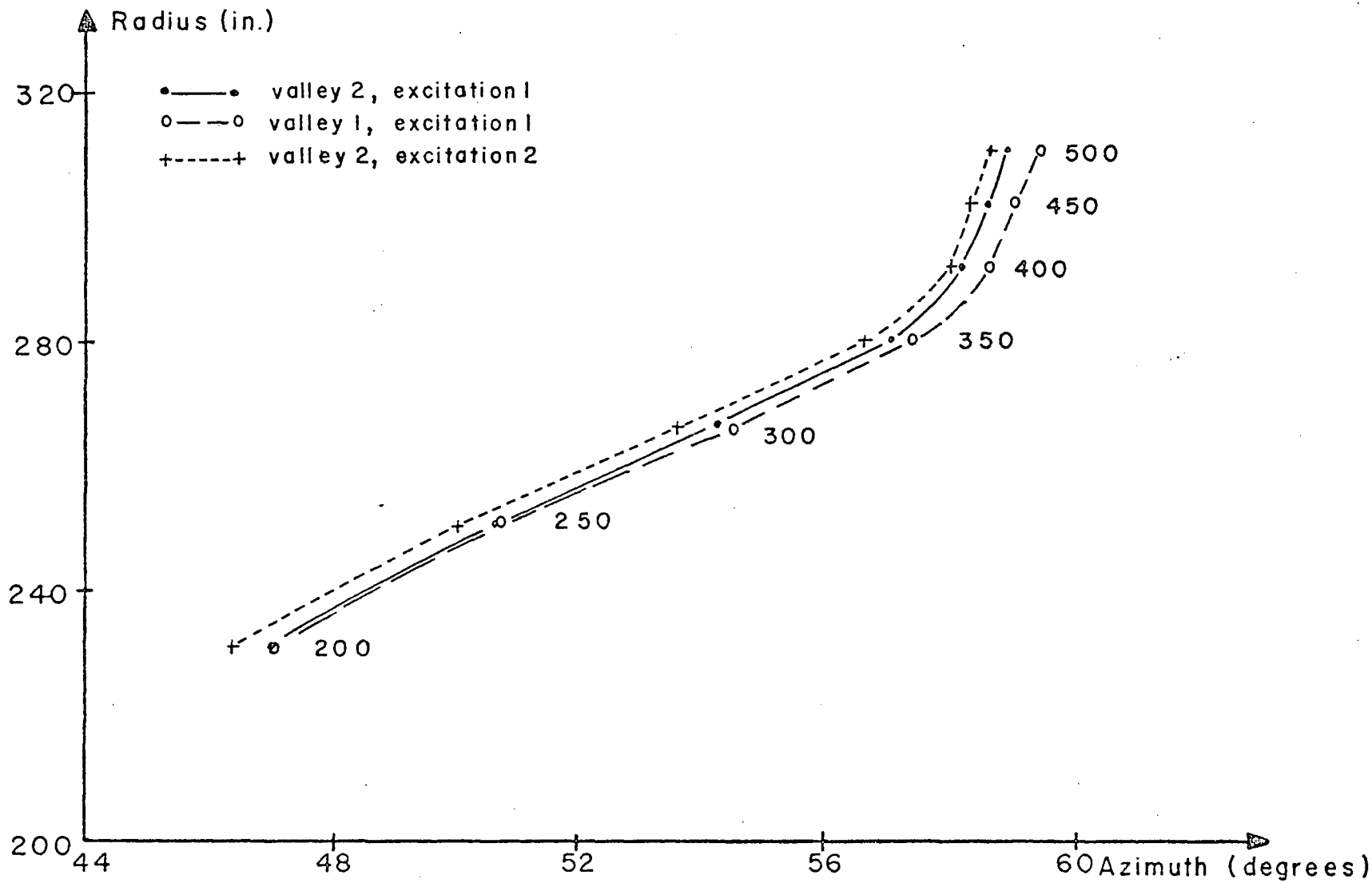

Fig. 3.5. Stripping foil locus from 200 to 500 Mev. for 2 extraction regions and 2 excitations of the cyclotron magnet.

A comparison was made of the internal field surveys before and after the combination magnet was put in place. The average value of the field at each radius, averaging over 60^{o}, were the same within 4 gauss. From the fourier analysis of the field the phase of the 6^{th} harmonic was within 0.03^{o} and the amplitude of this harmonic was within a few gauss. This parameter greatly influences the extraction properties.

When the combination magnet was excited and the effect on the cyclotron field checked a change of never more than 5 gauss was found, and the radial averages remained the same. In addition the presence of the combination magnet was seen not to change the field shape to any significant degree. When the stripping foil locus was determined the change in the locus was only $.01^{o}$ and .1 in. full scale.

The field profile of the combination magnet was unaltered by the presence of the excited cyclotron magnet, however the magnitude of the field was. When there was no excitation of the combination magnet a maximum field of -30 g. was found. Fig. 3.6 shows the excitation curve of this bending magnet when isolated and when next to the excited and unexcited cyclotron magnet. It was found that the return yokes of the combination magnet were saturating due to the fringe field of the cyclotron, and thus reducing the efficiency of the magnet.

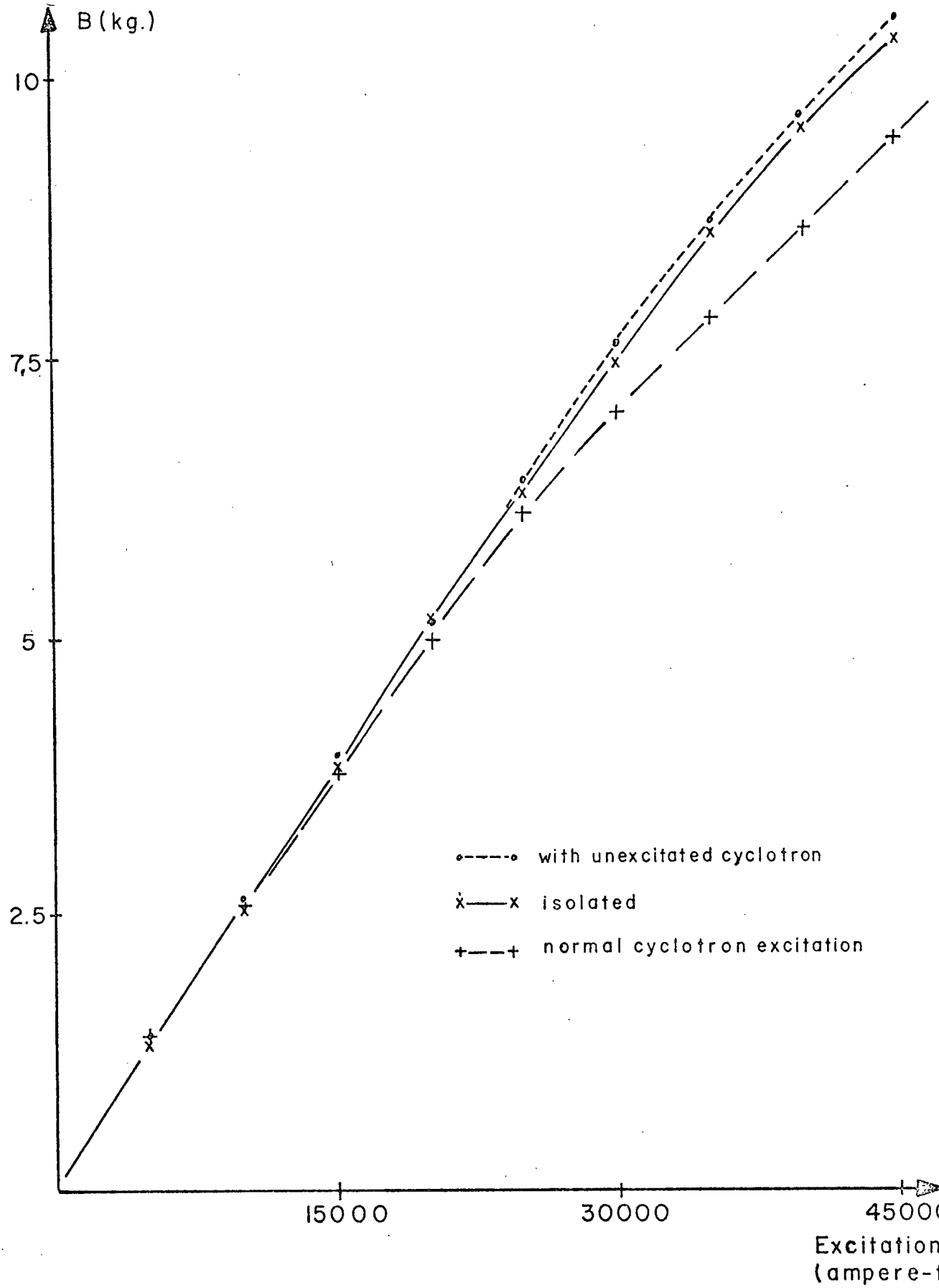

Fig. 3.6. Excitation of the combination magnet.

Since a maximum field of about 10 kg. is needed to bend the low energy beam, there will be a problem obtaining this energy of beam. Work is being done to solve this problem.

The presence of the combination magnet does not alter the characteristics of the fringe field so a hard edge approximation may be used to superimpose the combination magnet data on the fring field data.

3.6 Conclusions

It was decided that a maneuverability of 1^{o} and 1 in. would be necessary in the mechanism that supports the stripping foil. That it would be sufficient to survey one extraction region of the cyclotron and that the combination magnet would not significantly alter the beam orbits inside the cyclotron. But the combination magnet would have to be modified in order to extract any beam of energy less than 250 Mev.

4. THE TRIPLE HALL PROBE

4.1 The Device

4.1.1 Introduction

A method for locating the mean magnetic surface of an AVF cyclotron was developed and tested on the 1/20 scale model of the cyclotron magnet[11]. This technique proved to be capable of a precision of 0.010 in. Three Hall plates, mounted vertically above each other, see fig. 4.1, were used to provide a measure of $\frac{\partial^2 B_z}{\partial z^2}$. Since the median plane is defined by the surface where $\frac{\partial B_z}{\partial z}$ is zero, it can be determined from the equation

$$a = \frac{B_u - B_l}{2\,d\,\frac{\partial^2 B_z}{\partial z^2}} \qquad (4.1)$$

where B_u and B_l are the fields measured by the upper and lower Hall probes respectively. Thus the 3 Hall plates provide all the information required.

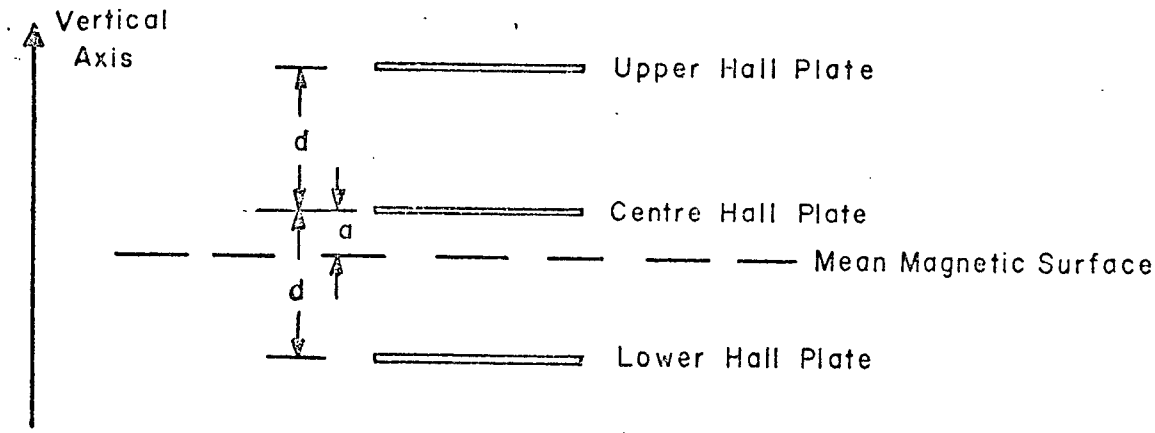

Fig. 4.1. Layout of the T.H.P. as used to measure the median plane.

It was found from the previous measurements that $\frac{\partial^2 B_z}{\partial z^2}$ often passed through zero on the circumference for most radii. That is there were many singularities in the value of a. In addition, from a series of communications between G. H. Mackenzie and B. Hedin of Cern, it was decided that what was of real interest was a complete knowledge of B_R, B_θ and $\frac{\partial B_z}{\partial z}$. A direct measurement of any one of these can in principle yield the others θ. A technique was determined by G. H. Mackenzie for the determination of any two of these quantities from a survey of the third.[12] The question arose whether it was better of measure the components directly or use a $\frac{\partial B_z}{\partial z}$ survey. Great difficulties have been encountered when trying to measure a small component of field in the presence of a large transverse component. One device for this purpose, the 'Russian Pendulum' uses a Hall plate which is held at a small angle θ to the verticle, see fig. 4.2. The

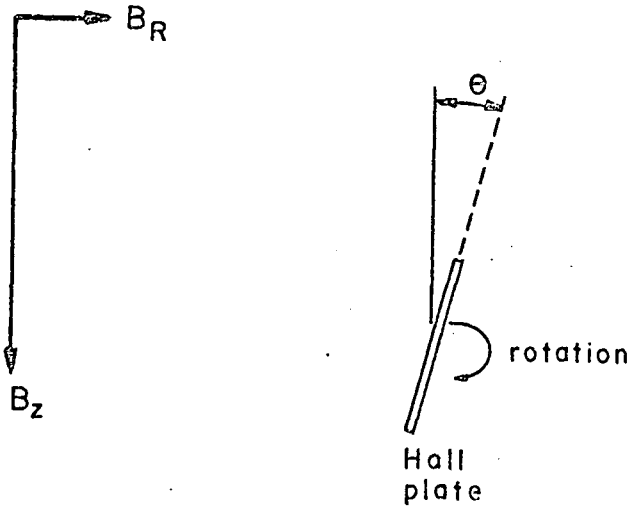

Fig. 4.2. Orientation of a Hall plate as used in a 'Russian Pendulum'.

Hall plate is rotated 180° and B_R is found from the sum of the readings before and after the rotation. Since the Hall plate reads a component $B_z\Theta$ as well as B_R, to measure a 5 gauss component of field to within 10% requires that Θ not change by more than 6.0×10^{-3} degrees in a B_z field of 5kg. In addition there are also non-linear effects taking place when a Hall plate is in such a large transverse field.[14] Table 4.1 shows the change in the effective angle of a BH701 Hall prove, produced by Bell Inc., as a function of the transverse field B_z.

B_z (kg)	ϕ_Θ^L (deg)	ϕ_Θ^C (deg)	ϕ_Θ^U (deg)
1.252	0.67	1.92	-0.41
2.019	0.88	2.07	-0.43
3.008	1.01	2.13	-0.48
4.011	1.07	2.17	-0.50
5.017	1.11	2.19	-0.51
5.976	1.13	2.20	-0.52
7.034	1.16	2.21	-0.52
10.072	1.78	2.22	-0.54

Table 4.1. Change in the effective angle with the Hall plates rotated 90° from the horizontal.

In our case the focusing forces are spread over large regions, so the horizontal field may be any mixture of B_R and B_θ. This means that the devide must be aligned in another degree of motion so that the presence of a B_θ component will not interfer with the measurement of a B_R component and vice-versa. This further complicates the measurement of these horizontal components.

For the measurement of $\frac{\partial B_z}{\partial z}$, as will be shown, the tolerances of the alignment of the Hall probes are more acceptable and the problem of solid state effects is avoided since B_z is measured. For these reasons it was decided to build a Triple Hall Probe (T.H.P.). This probe was used to provide a measurement of the median surface and the radial and azimuth components of the cyclotron field. The orbit code CYCLOPS was also mofified to accept this data and calculate the vertical equilibrium orbits as a function of energy. This provides the vertical position z and the vertical component of the momentum P_z, as a function of energy and azimuthal position.

4.1.2 Theory of Measurement

Using an expression, suggested by M. M. Gordon[15], for the scalar potential of the field in the cyclotron

$$\Psi = C - \frac{z^2}{2} \nabla^2 C + \frac{z^4}{4!} \nabla^4 C \cdots + z\beta - \frac{z^3}{3!} \nabla^2 B \quad (4.2)$$

where $B(R,\theta)$ describes the symmetric and $C(R,\theta)$ antisymmetric

parts of the field. The components of the field can be shown from $\vec{B} = \nabla\Psi$ to be given by

$$B_z = B_{z_o} - z\nabla^2 C - \frac{z^2}{2}\nabla^2 B + \frac{z^3}{3!}\nabla^4 C \ldots \quad (4.3)$$

$$RB_\theta = \frac{\partial C}{\partial \theta} + z\frac{\partial B}{\partial \theta} - \frac{z^2}{2}\frac{\partial}{\partial \theta}(\nabla^2 C) \ldots \quad (4.4)$$

$$B_R = \frac{\partial C}{\partial R} + z\frac{\partial B}{\partial R} - \frac{z^2}{2}\frac{\partial}{\partial R}(\nabla^2 C) \ldots \quad (4.5)$$

In the plane of measurement z is zero so

$$\nabla^2 C = -\frac{\partial B_z}{\partial z} \quad (4.6)$$

We may solve this equation for $C(R,\theta)$ using a Greens function technique and a measured map of $\frac{\partial B_z}{\partial z}$ and thus determine B_R and B_θ. These components are used by the equations[12] in CYCLOPS.

4.1.3 Tolerances

The accuracy of the results for B_R and B_θ depends on the quality of the function

$$f(R,\theta) = -\frac{\partial B_z}{\partial z} \quad (4.7)$$

It was hoped to measure $\frac{\partial B_z}{\partial z}$ to 1 g./in. In the T.H.P. there are 4 kinds of misalignment; (1) the vertical separation of the plates, (2) the displacement of the magnetic centre of the Hall plates above each other, and (3) & (4) the tilts of the Hall plates with respect to

the plane of measurement. The Hall plates may be tilted with respect to a radius, the effective angle denoted by ϕ_R, and thus be sensitive to B_R components; and may also be tilted with respect to the azimuth, denoted by ϕ_θ, and so be sensitive to B_θ components.

To provide a 1 g./in. accuracy in $\frac{\partial B_z}{\partial z}$ in our 1/10 scale T.H.P., each Hall plate must be correct to 0.7 gauss. And if for each probe the 4 sources of error contribute equally, then each may be the source of only a 0.35 gauss error. It is extremely difficult to construct a T.H.P. that will immediately satisfy these tolerances. However if the 4 above mentioned misalignments are known then corrections to the measured data can be made to obtain the desired accuracy.

In the 1/10 scale model the transverse gradients $\frac{\partial B_z}{\partial R}$ and $\frac{1}{R}\frac{\partial B_z}{\partial \theta}$ may be as high as 250 g./in. This implies that the magnetic centres be known to within 0.0014 in. The allowed tilt of the Hall plates are determined by the horizontal components of the field for the upper and lower Hall probes, and the sine of their angular misalignment. These errors may be approximated by $d\frac{\partial B_z}{\partial R}\sin\phi_R$ and $\frac{d}{R}\frac{\partial B_z}{\partial \theta}\sin\phi_\theta$. This leads to a tolerance of $\pm 0.2^o$ for our 1/10 scale model. Finally, since $\frac{\partial B_z}{\partial z}$ is determined from the difference formula $\frac{B_u - B_l}{2d}$ then d must be known to 0.005 in.

4.2 Construction and Calibration

A T.H.P. was built, see fig. 4.3, using three BH701 Hall plates. They were mounted in the 3 slots shown. The block containing the Hall probes was brass and had a heating element wound around a spool shown on the left side of the cross-section in fig.4.4. The block was machined so the separation of the probes was 0.5 $\pm$0.002 in. The entire block was encased in a plexiglass box with walls 1/8 in. thick. A temperature controller kept the temperature constant to 0.1^{o} C. so that temperature effects were negligible. The probes were calibrated to 1 gauss with the previously mentioned NMR digital gaussmeter.

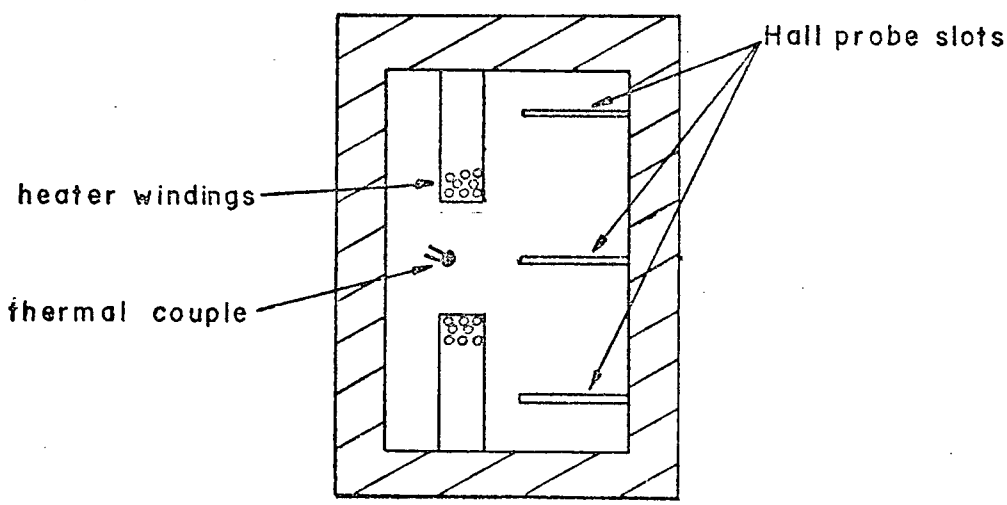

Fig. 4.3. Design of the 1/10 scale model T.H.P.

To measure the alignment of the probes, the calibration magnet referred to in chapter 2, was used in conjunction with a milling table having a travel 8 by 4 in. and accurate to one thousandth of an inch. Fig. 4.4 shows the orientation of the table with respect to the calibration magnet. The T.H.P. was mounted tightly in the end of an aluminum U shaped channel, the other end was bolted to the milling table. The L bar enabled us to reposition the channel to within 0.001 in. and rotate the T.H.P. $\pm 90^{o}$ about the x axis. Using a precision bubble level with a 12 in. long base, the milling table was determined to be vertical within 0.02^{o}, and level to within 0.1^{o}.

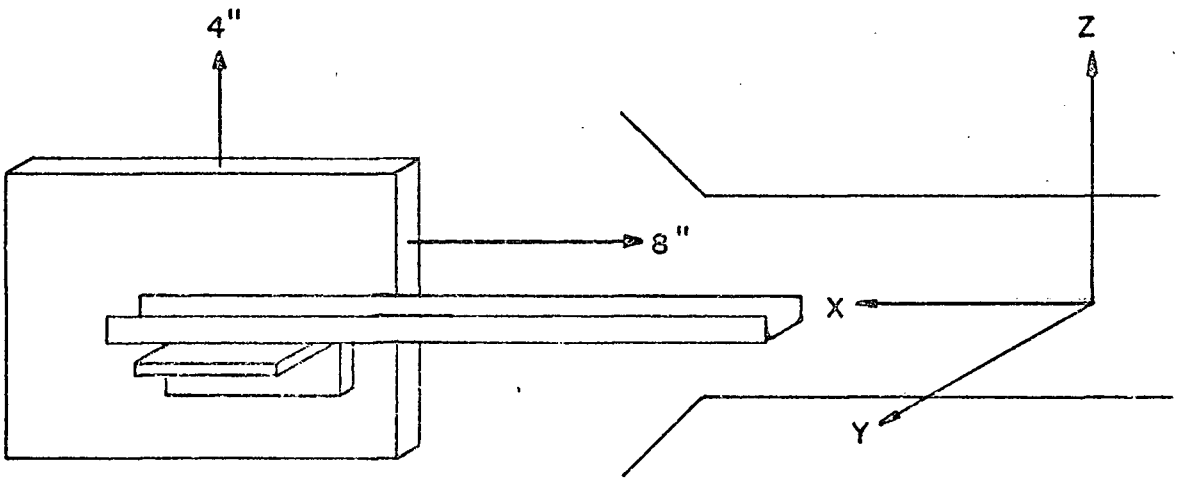

Fig. 4.4. Milling table and U channel in position with respect to the calibration magnet.

To first measure the $\emptyset_{\theta}$'s of the 3 Hall plates we placed the T.H.P. in the flat region of the field, measured B_z then rotated the channel $+90^{o}$ and measured

the effective B_y, then -90° and repeated the measurements. This was done for several excitations. Table 4.1 gives the results for anti-clockwise rotation and table 4.2 shows the results for clockwise rotation. As before we see the same anomalous effects.

B_z(kg.)	ϕ_θ^L (deg)	ϕ_θ^C (deg)	ϕ_θ^u (deg)
1.244	-1.06	-2.58	0.28
2.512	-1.14	-2.44	0.39
3.995	-1.19	-2.38	0.46
5.506	-1.22	-2.35	0.49
6.986	-1.23	-2.34	0.51
10.008	-1.24	-2.30	0.53

Table 4.2. Effective angle of the Hall plates rotated 90° from the horizontal, as a function of B_z.

To determine what the correct ϕ_R's are in the second manner we used the milling table to move the central Hall plate ½ in. above and below the geometric median plane (z=0), see fig. 4.5. If this Hall plate is tilted by an angle α then the difference in the two readings B is given by

$$\Delta B = 2\Delta z \quad \frac{\partial B_x}{\partial z} \quad \sin\alpha \qquad (4.8)$$

Using eqn. A.4 we get

$$\sin\alpha = \Delta B/2\Delta z \quad \frac{\partial B_z}{\partial z} \qquad (4.9)$$

Also if two Hall plates, such as the centre and lower are in the same position above and below the median plane then the relative angle between them can be found using the same technique.

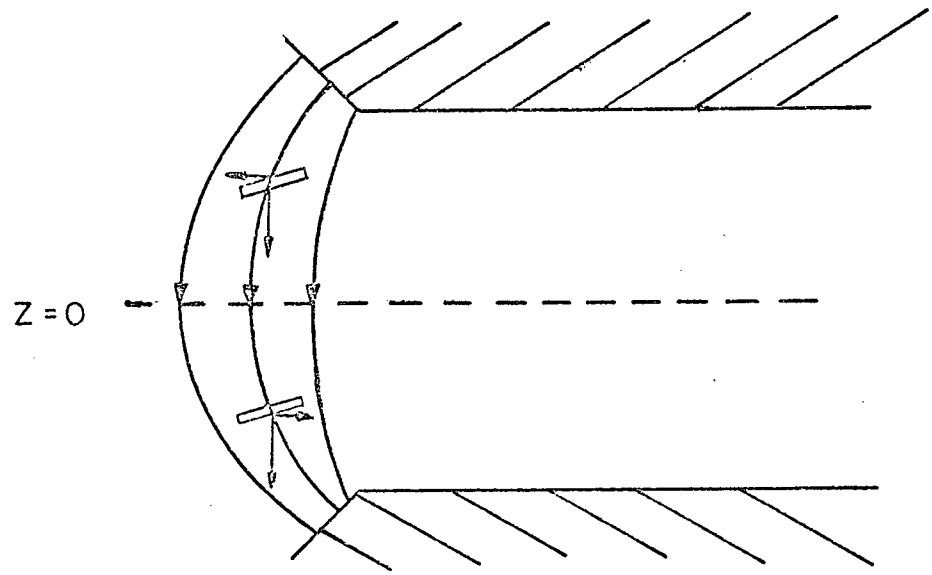

Fig. 4.5. Effect of measurements taken at equal displacements above and below the median plane in the fringe field of the calibration magnet.

For this method to be accurate $\frac{\partial B_z}{\partial z}$ should be constant so that B_x can be closely approximated by $\Delta z \frac{\partial B_x}{\partial z}$. Unfortunately, it was found that in the region where $\frac{\partial B_z}{\partial x}$ was constant there was a large assymetry in the field due to the deflection of one of the coils of the calibration magnet. In fact was as large as 35 g./in. This prevented a measurement of the tilt ϕ_θ^c of the centre probe. Measurements of the relative angle between two probes ½ in. apart were still possible, however the uncertainty of positioning,

0.001 in. in the z and x directions imply a 3 gauss uncertainty in the difference of fields. Also, latter it was found that the milling table rocked back and forth as the T.H.P. was moved along the x axis. From this another 3 gauss uncertainty was created such that the relative angles could be incorrect by 30%. Table 4.3 summarizes the results of 2 sets of these measurements.

$\phi_\theta^C - \phi_\theta^L$ (deg.)	$\phi_\theta^C - \phi_\theta^U$ (deg.)
1.7	3.3
0.0	3.2
1.0	2.9
0.1	2.8
AVG. 0.7	3.05

Table 4.3. Measurement of the relative tilt of the upper and lower Hall plates with respect to the centre plate.

To overcome this problem a third method was devised that gave ϕ_θ independently for each of the 3 probes. An aluminum wedge with an angle of inclination of $15^{o\pm}$ 0.05 was constructed. A short piece of aluminum U channel was bolted to the wedge and the T.H.P. placed in the channel. This whole apparatus was then placed on a pole piece in the flat field region, as shown in fig. 4.6. The T.H.P. can be rotated so that it points in the opposite direction,

then the difference of the results gives B according to

$$\Delta B = \Leftrightarrow 2B_z \sin 15. \sin \phi_\theta \qquad (4.10)$$

Table 4.4 summarizes the results of this technique.

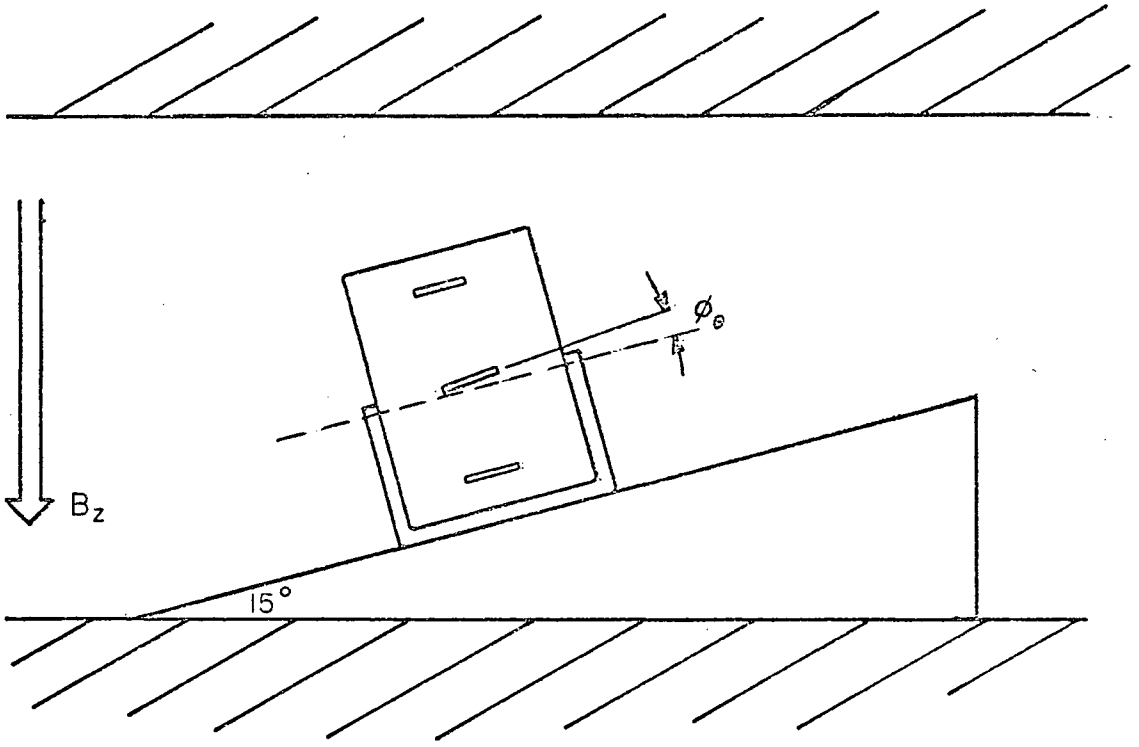

Fig. 4.6. T.H.P. mounted on the wedge for measurement of ϕ_θ. Apparatus is in the flat region of the field.

The results of the third method are expected to be the most reliable and so it was concluded that ϕ_θ^u was 1.3°, ϕ_θ^c was 2.6°, and ϕ_θ^L was $-.1^\circ$. These are precise to $\pm 0.15^\circ$.

B_z (kg.)	ϕ_θ^u (deg.)	ϕ_θ^c (deg.)	ϕ_θ^L (deg.)
1.372	1.15	2.6	-.0
3.109	1.15	2.5	-.13
5.013	1.4	2.7	-.0
6.132	1.4	2.6	-.09
AVG.	1.28	2.60	-.05

Table 4.4. Measured angles using the aluminum wedge.

To measure the angles ϕ_R it wasn't possible to rotate the T.H.P. through 90^o as before since it was longer then the gap width of the calibration magnet. Measurements of the relative tilts were made in the fringe field as described in fig. 4.5, but were of such poor quality that the attempt was abandoned. The wedge technique however could be used after the channel with the T.H.P. was rotated 90^o from the position shown in fig. 4.6. The results are given in table 4.5. Since

B (kg.)	ϕ_R^u (deg.)	ϕ_R^c (deg.)	ϕ_R^L (deg.)
1.372	-.2	-.03	1.0
2.929	-.3	-.03	1.0
5.014	-.3	-.06	1.1
6.032	-.3	-.08	1.1
AVG.	-.28	-.05	1.05

Table 4.5. Measured angles using the aluminum wedge.

the field values are precise to 1 gauss then the implied tolerance on these results is $\pm 0.01^{o}$.

Now to determine the displacement of the magnetic centres we used a technique that involved moving the T.H.P. through the fringe field again, where $\frac{\partial B_z}{\partial x}$ was constant. First the T.H.P. was raised so that the lower Hall plate was on the geometrical plane of symmetry and a record of B_z versus x was made for each Hall plate, the T.H.P. was lowered ½ in. and B_z versus x recorded as before, and lastly the same was done with T.H.P. ½ in. even lower. The data could be interpolated to give the value of x for each plate at which it passed through the same B_z, where z is zero. The difference in x should then give the separations of the magnetic centres of the Hall plates. At the same time this was done we also got a record of B_z versus x for the upper and centre hall probes, ½ in. above the median plane and for the lower and centre hall probes ½ in. below the median plane. These give a check on the separations. To double check our results, we turned the T.H.P. about, so it pointed in the opposite direction, and repeated the measurements.

When this was first done the separations appeared to be about 0.010 in. but varied considerable with different z and when the T.H.P. was reversed in direction. In fact the apparent order of the probes changed when the T.H.P. was turned about. It was thought that one source

of this dilemma could be from the probe's sensitivity to the horizontal component of the field. In fact, for z of $\pm\frac{1}{2}$ in. B_x is so large that displacements measured at these heights had to be discarded. However on the median plane this should not have been such a problem. It then became apparent that the T.H.P. must be on an angle. From fig. 4.7 we see that the apparent separation is given by

$$s = d \sin\alpha + S \cos\alpha \tag{4.11}$$

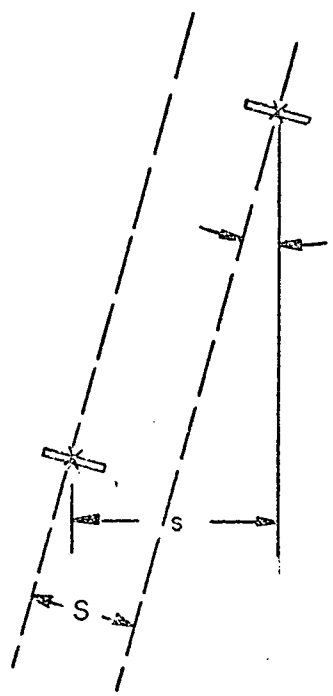

Fig. 4.7. Relative position of 2 Hall plates when the T.H.P. is tilted by an angle α. S Represents the true separation and s the apparent separation.

where S is the true separation, α is the tilt of the T.H.P., and d is the distance vertically between the Hall plates, either ½ in. or 1 in. Since the T.H.P. was rotated 180° about face the error due to d sin α was introduced twice. 2d sin α May easily be of the order of 0.010 in. so it was no surprise that our earliest attempts failed. However with this understanding it was possible to deduce the true separations as well as the value of α. Figures 4.8 and 4.9 illustrate the

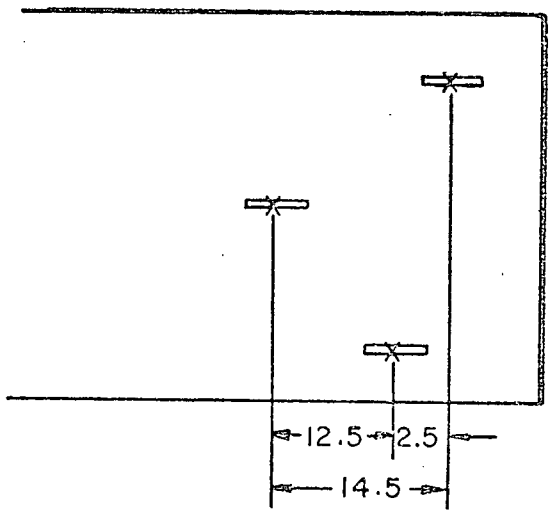

$\sin \alpha = 0.009. \mp 0.002$

Fig. 4.8. First measurement of the separation of the magnetic centre in the radial direction. Distances in thousandths of an inch.

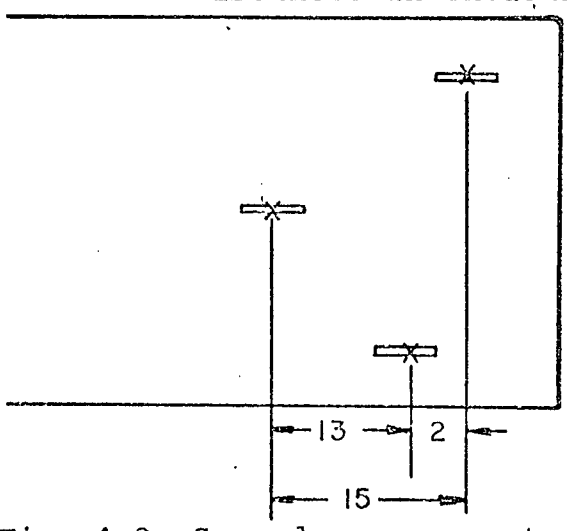

$\sin \alpha = 0.010 \pm 0.002$

Fig. 4.9. Second measurement of the separation of the magnetic centres in the radial direction. Distances are in thousandths of an inch.

results of 2 measurements made, all units are in thousandths of an inch. The displacements were consistent to within 0.001 in. which was the limit of measurement. We now saw that α was about 0.6° and that our measurements were very sensitive to a tilt of the T.H.P. We re-measured the tilt of the U channel with more care and indeed found that it was 0.6°. The apparatus was re-aligned and the measurement repeated. The results are shown in fig. 4.10. The results this time were consistent

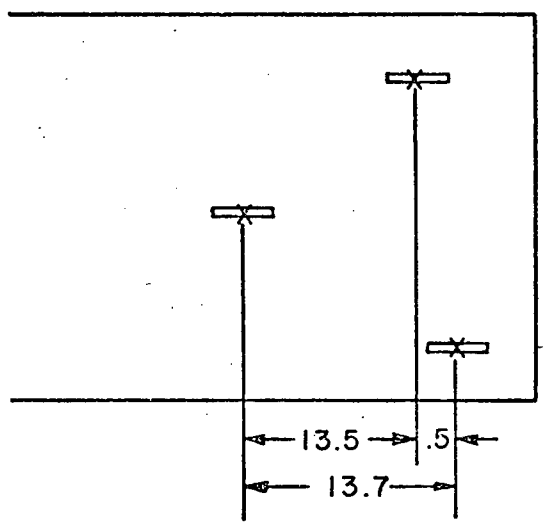

$$\sin \alpha = 0.0015 \pm 0.001$$

Fig. 4.10. Improved measurement of the separation of the magnetic centres in the radial direction. The distances are in thousandths of an inch.

and so it was concluded that fig. 4.10 gave the correct configuration.

These measurements were repeated with the Hall probe perpendicular to the x axis so that the separation of the magnetic centres in the azimuthal direction could

be determined. Fig. 4.11 illustrates the results of our only measurement.

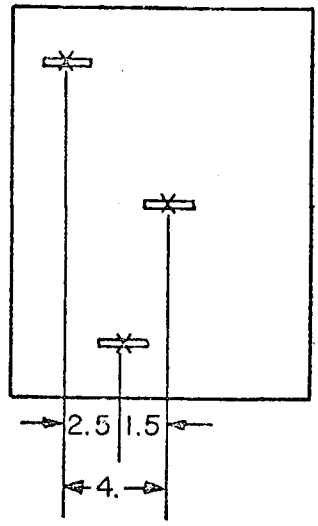

$$\sin \alpha = 0.001 \pm 0.0005$$

Fig. 4.11. Front end view showing the separation of the magnetic centres of the Hall plates in the azimuthal direction. Distances are in thousandths of an inch.

Thus we have determined three of the mis-alignments within the tolerances demanded. Using these values the results of the upper and lower Hall plates can be corrected to give values of α to nearly the desired precision. In the survey of the full scale cyclotron magnet the angular tolerances would remain the same but the length tolerances would relax. That survey will also be done with the benefit of the experience gained here and consequently should be a much more accurate one.

4.3 Measurements and Results

First to check the performance and sensitivity of the T.H.P., it was drawn through the field of the calibration magnet along the x axis. First the survey was done from the centre out through the fringe field of the calibration magnet to determine its properties. This was when the assymetry in its fringe field was discovered. Then we repeated the survey with an iron bar, 1/8 by ½ by 10 in. parallel to the y axis flat against the top pole piece and 6 in. in from the front edge of the pole. In each case the T.H.P. was centred so that the central Hall plate was within 0.010 in. of the geo metric median plane. First order corrections were made using the results of the last section. Fig. 4.12 shows the position of the median surface a as given by eqn. 4.1, with the iron bar in place. It can be seen that the quantity a of eqn. 4.1 has 4 singularities in the region surveyed.

Fig. 4.13 shows the $\frac{\partial B_z}{\partial z}$ as measured with the T.H.P. It is compared to the results of a 2 dimensional relaxation program MARELAX2D[16]. Fig. 4.14 gives the horizontal component of the field as predicted by this relaxation program and as obtained from the data. In this particular case eqn.'s 4.5 and 4.6 reduce to

$$B_x = \int_{x_i}^{x} \frac{\partial B_z}{\partial z}(x^1)\, d x^1 \qquad (4.12)$$

where x_i is a point along the x-axis where $\frac{\partial B_z}{\partial z}$ is zero. So the measurements were integrated using Simpson's rule to give $B_x(x)$.

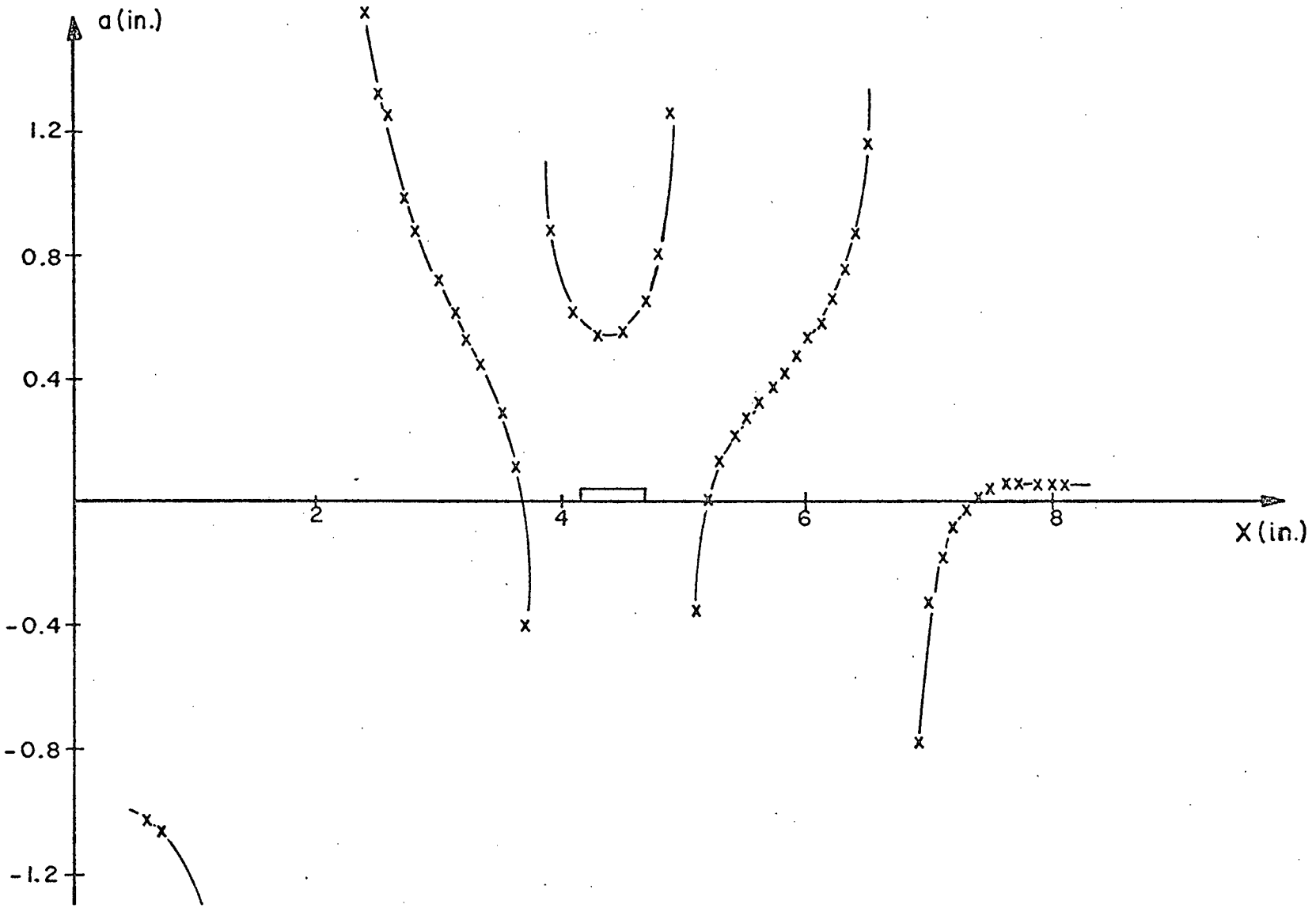

Fig. 4.12. Position of the mean magnetic surface with an iron bar on one pole piece.

To make the comparison with the relaxation program the error in $\frac{\partial B_z}{\partial z}$ due to the fact that the separation of the Hall plates was not small compared to the gap width, had to be corrected. By considering a Taylor series for B_z about the median plane, z=0 (see Appendix A), it can readily be shown that

$$\left(\frac{\partial B_z}{\partial z}\right)_o = \frac{B_u - B_L}{2\Delta z} + \frac{(\Delta z)^2}{3!}\left(\frac{\partial^3 B_z}{\partial z^3}\right)_o + \ldots \quad (4.13)$$

In appendix A it is shown that

$$\frac{\partial^3 B_z}{\partial z^3} = \frac{\partial^2}{\partial x^2}\left(\frac{\partial B_z}{\partial z}\right) \quad (4.14)$$

which may be determined from the measured data. Thus we see that the measurements require a third order correction. This was made to the data in fig. 4.13 before integrating. The correction meant in fact about a 20% decrease in the values for $\frac{\partial B_z}{\partial z}$.

For the TRIUMF cyclotron a large web of iron beams are used to support the top of the pole pieces and provide for the raising of the top half of the magnet. There was some concern that this large asymmetry in the distribution of iron about the magnet would cause a shift in the vertical equilibrium orbits. To study the effect of the I beams in the support structure bars of iron were placed against the I beam to increase the effective magnetization. Surveys of the 1/10 model magnet field were made before and after, and the results compared. The iron bars used

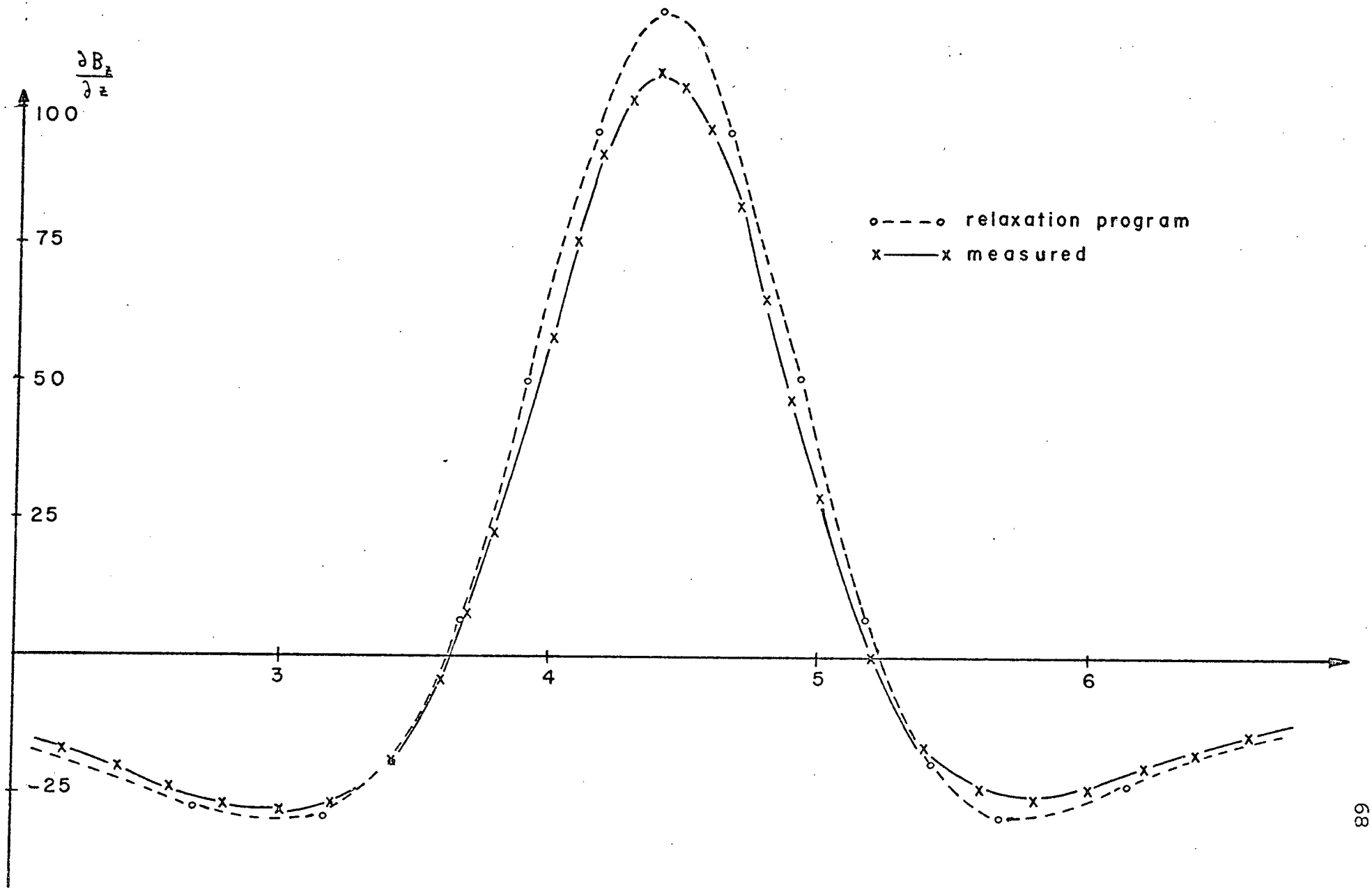

Fig. 4.13. $\frac{\partial B_z}{\partial z}$ For the iron bar on a pole of the calibration magnet.

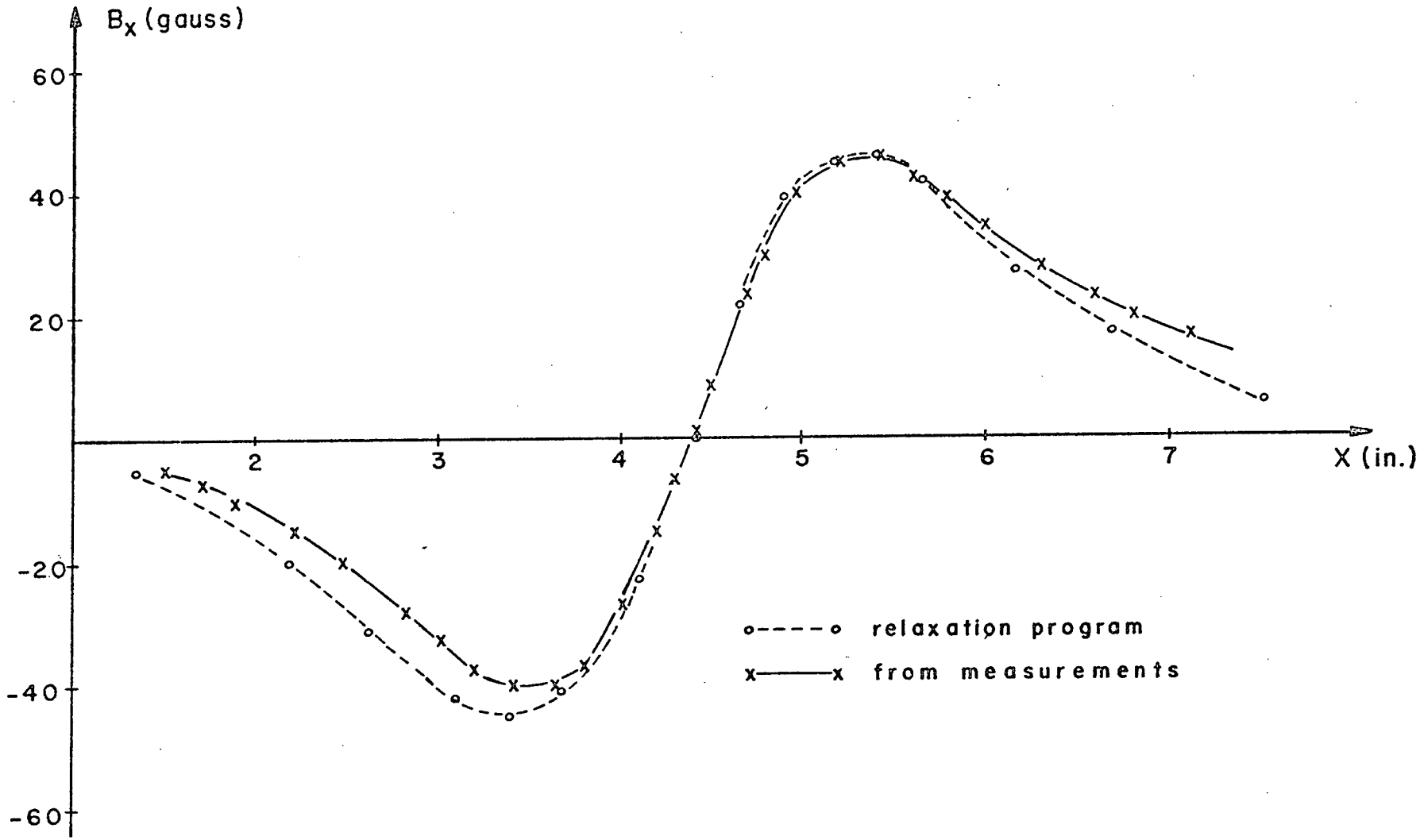

Fig. 4.14. B_x For the iron bar in the calibration magnet.

amounted to ½ the volume of iron used in an I beam. In none of the tests was it possible to distinguish any change due to these bars.

A circular disc 10 in. in diameter and 0.31 in. thick was attached to the surface of a pole piece at radius 170 in. and azimuth 73°. T.H.P. surveys were made with and without this disc. Fig. 4.15 gives the measured $\frac{\partial B_z}{\partial z}$ at 170 in. as a function of azimuth θ; as measured and as predicted by a dipole model. The data is actually the difference of the derivatives from the two surveys. The dipole model assumed the field of the disc was the shape of a dipole field but used the demagnetization factor determined numerically for a uniformly magnetized ellipsoid that approximated the shape of the disc. This factor was 10.5.

Fig. 4.16 gives B_θ from the dipole theory and as determined from a solution of eqn. 4.6.

The difference field was fed into the routine CYCLOPS. This program calculates the vertical equilibrium orbits over a 60° sector or any multiple thereof. Table 4.6 gives some results of CYCLOPS; z is the displacement of the beam vertically and p_z is the component of the momentum in the vertical direction. For this case the data over 60° was used assuming 6 fold symmetry, ie. each of the 6 sectors had such a disc on the top pole piece; the z and p_z are given along the 0° radian, which is in the middle

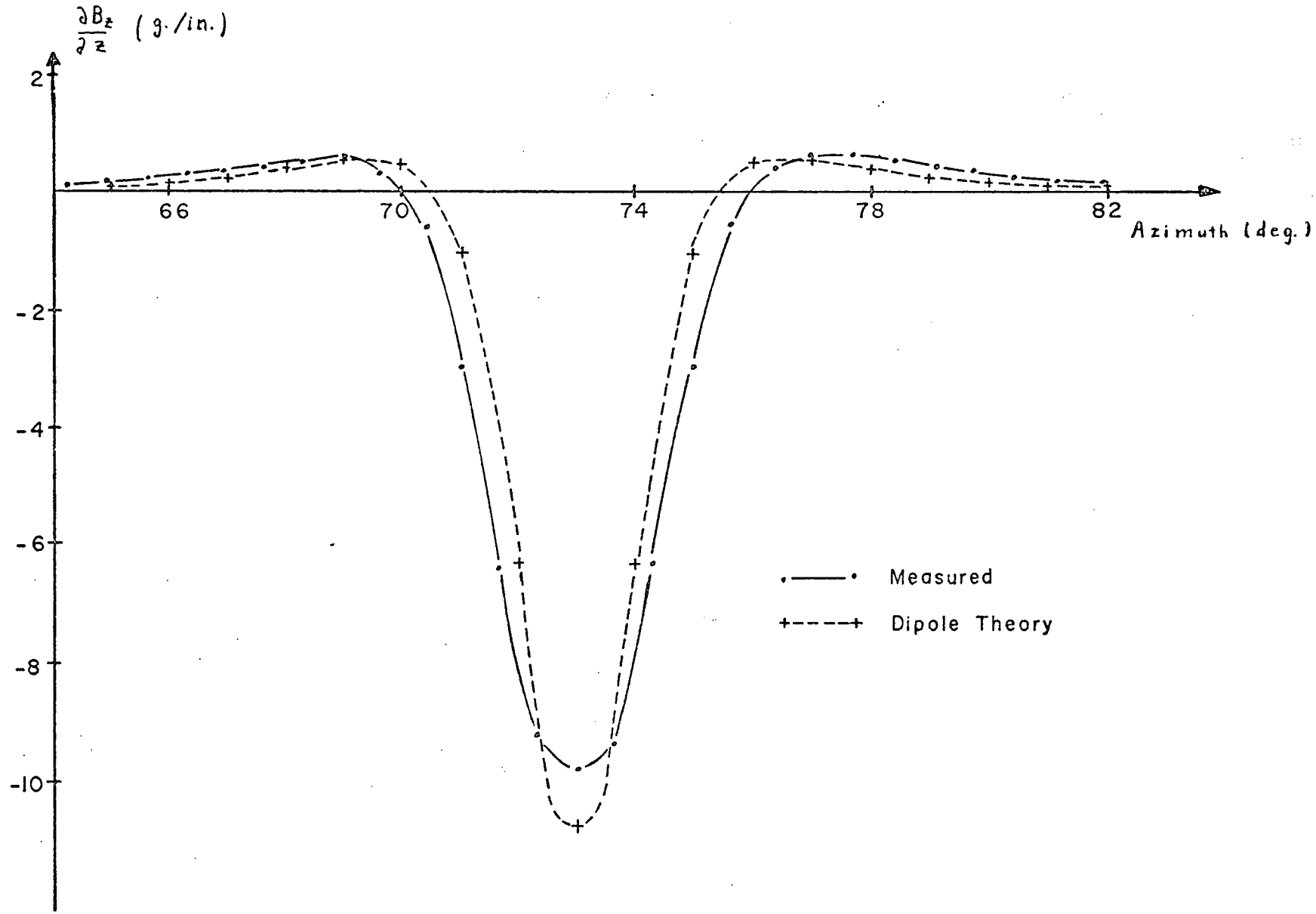

Fig. 4.15. $\frac{\partial B_z}{\partial z}$ For the disc on a pole face in the 1/10 scale cyclotron magnet.

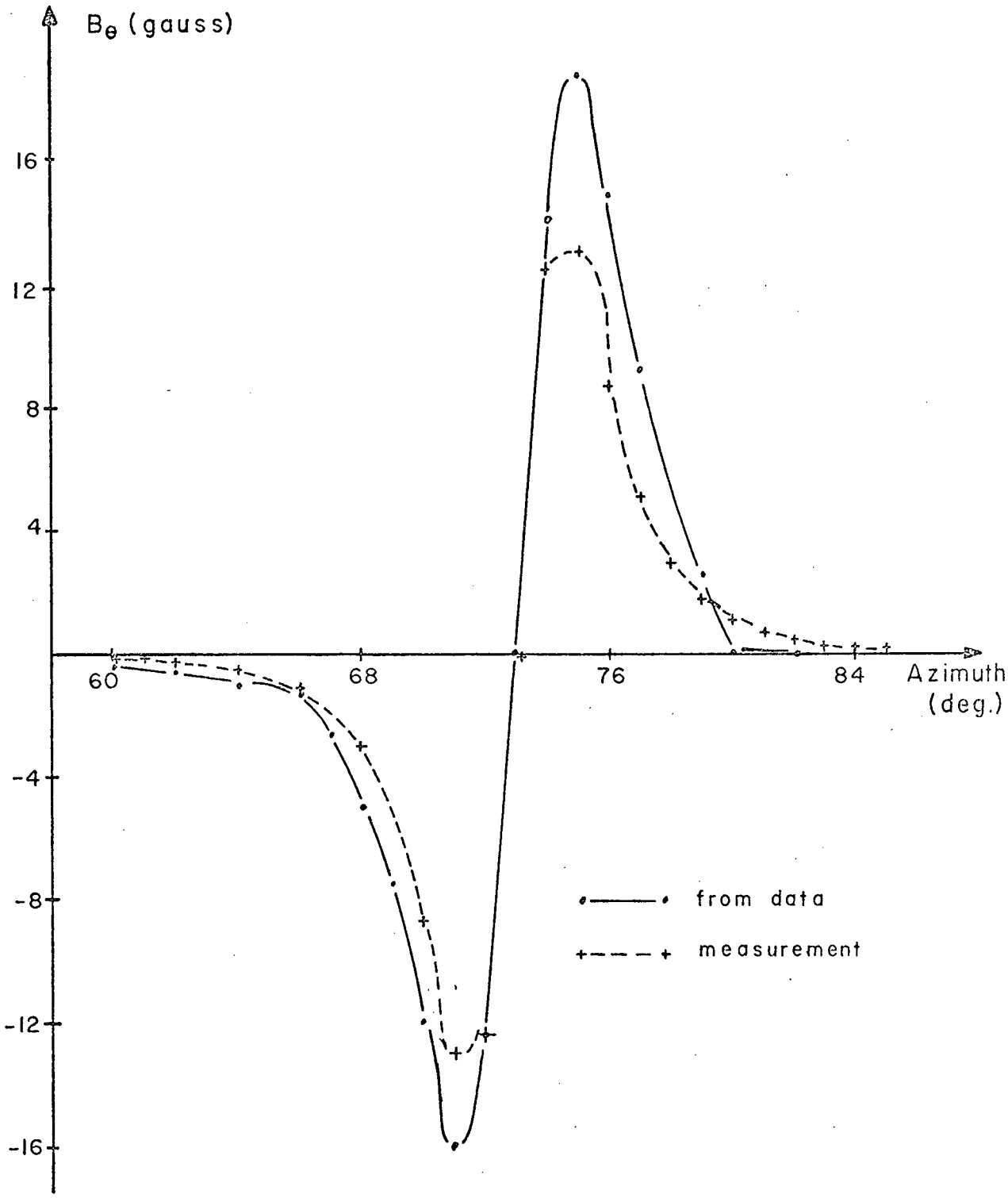

Fig. 4.16. B_θ For the disc on a pole face in the 1/10 scale cyclotron magnet.

ENERGY (Mev.)	R (in.)	PR (in.)	RAVE (in.)	NU(R)	NU(Z)	Z (in.)	PZ (in.)
70.0	146.51	1.2922	149.31	1.092	0.305	-0.122	-0.001
75.0	151.04	1.2780	153.97	1.097	0.301	-0.266	-0.004
80.0	155.37	1 2293	158.43	1.102	0.288	-0.511	-0.011
85.0	159.52	1.1334	162.70	1.108	0.278	-0.585	-0.020
90.0	163.52	0.9845	166.81	1.113	0.268	-0.144	-0.007
95.0	167.37	0.7798	170.77	1.119	0.256	0.710	0.047
100.0	171.07	0.5027	174.57	1.124	0.246	1.393	0.123
105.0	174.64	0.1357	178.23	1.129	0.235	1.522	0.170
110.0	178.11	-0.3150	181.78	1.135	0.223	1.239	0.169

Table 4.6. Effect on disc on the beam for equilibirum orbits at 5 Mev. increments. Momentum in cyclotron units.

of the valley just before the pole piece with the disc. These values represent the motion of the beam due to the disc alone, ie. they would be zero if the disc was not there. The beam is deflected downwards by the disc at radii less than 170 in.

Table 4.7 is an extended output of CYCLOPS for the same data as above. It shows the z motion of the beam as a function of azimuth for an orbit that passes nearly through the centre of the disc. The beam is deflected downwards then upwards by the disc.

Fig. 4.17 illustrates the effect of a 2 in. thick (full scale dimensions) shim added to the bottom edge of a pole piece but not to the top edge. The assymetry in

Theta (deg.)	R (in.)	PR (in.)	Z (in.)	PZ (in.)
2.0	167.46	5.12	0.711	0.044
4.0	167.69	9.38	0.712	0.040
6.0	168.04	13.51	0.713	0.034
8.0	168.53	17.35	0.714	0.023
10.0	169.13	20.72	0.715	0.006
12.0	169.82	23.30	0.715	-0.021
14.0	170.59	24.47	0.713	-0.066
16.0	171.36	23.58	0.710	-0.110
18.0	172.07	20.93	0.706	-0.126
20.0	172.69	17.54	0.703	-0.119
22.0	173.20	14.01	0.699	-0.107
24.0	173.59	10.37	0.696	-0.093
26.0	173.86	6.69	0.693	-0.072
28.0	174.02	3.02	0.691	-0.049
30.0	174.06	-0.69	0.690	-0.027
32.0	173.98	-4.40	0.689	-0.009
34.0	173.77	-8.10	0.689	0.005
36.0	173.45	-11.83	0.690	0.020
38.0	173.01	-15.49	0.690	0.035
40.0	172.46	-19.05	0.692	0.050
42.0	171.80	-22.25	0.694	0.065
44.0	171.05	-24.15	0.696	0.700
46.0	170.28	-24.04	0.698	0.064
48.0	169.54	-22.21	0.700	0.057
50.0	168.88	-19.34	0.702	0.053
52.0	168.33	-15.85	0.703	0.051
54.0	167.90	-11.96	0.705	0.049
56.0	167.59	-7.83	0.706	0.049
58.0	167.41	-3.56	0.708	0.048
60.0	167.37	0.77	0.709	0.046

Table 4.7. Vertical motion of the beam with azimuth; the disc is centred about 12°. Momentum in cyclotron units.

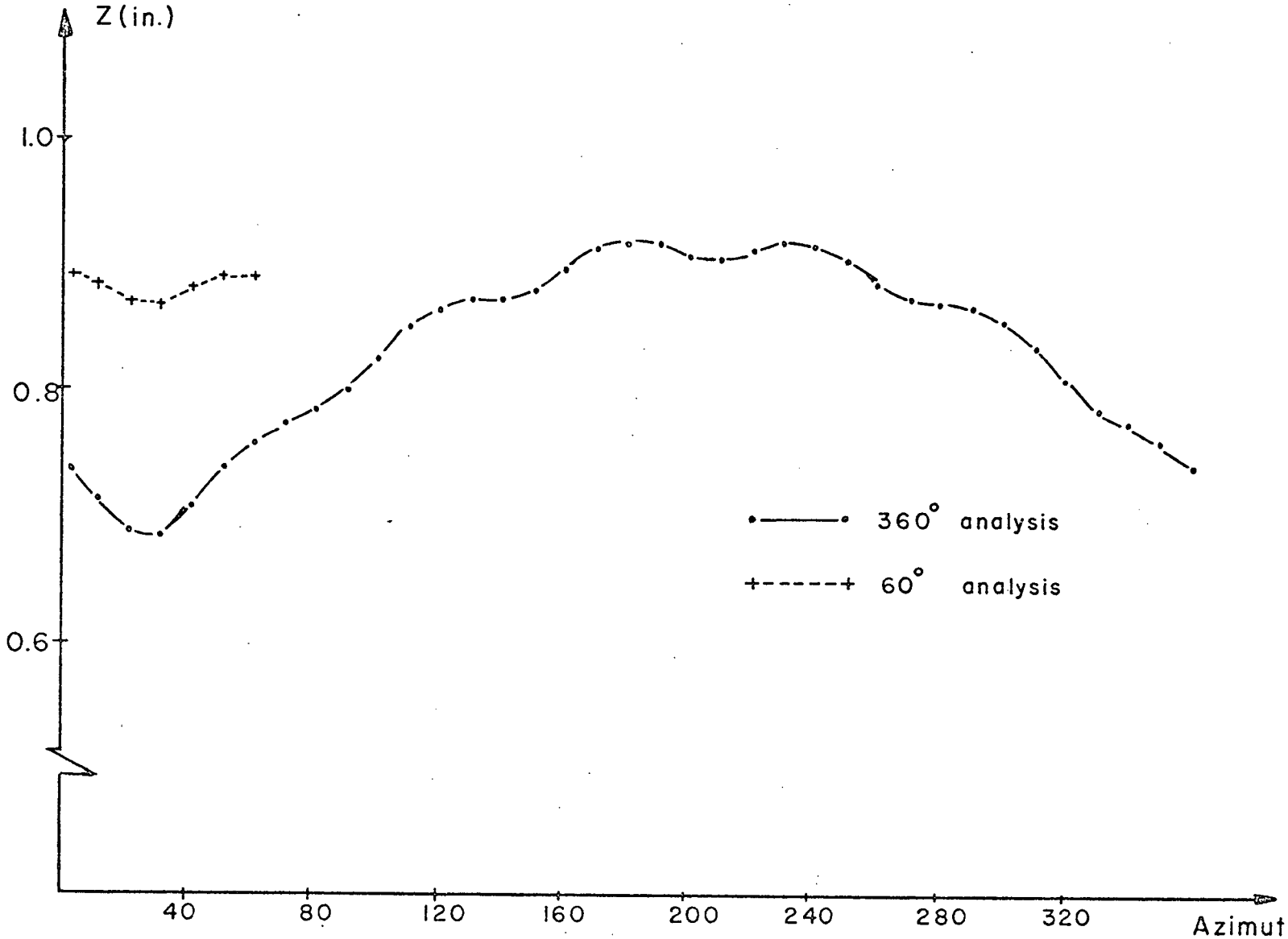

Fig. 4.17. Vertical motion of the beam at 115.5 in. due to a 2 in. shim on the edge of one bottom pole piece.

the field causes a vertical deflection in the beam. The 360° analysis treats the field with this shim on just 1 of the 6 pole pieces; where the 60° analysis assumes that a .033 in. shim was added assymetrically to each pole piece; the motion shown would be repeated over every 60°.

4.4 Conclusion

Our measurement of $\frac{\partial B_z}{\partial z}$ seemed to be as precise as required for localized field errors. From the deflection of the beam due to the disc and shim, it appears that we could detect the presence of an assymetric shim or lump in a pole piece of at least 10 times smaller than those used in our tests. Since the full scale survey will be more precise than this one, we should be able to determine the vertical motion of the orbits within a few tens thousandths of an inch for localized field errors.

5. TRIM AND HARMONIC COILS

5.1 Introduction

5.1.1 Purpose

The trim and harmonic trim coils are pairs of single current loops that can cause small changes in the magnetic field of the cyclotron. These coils are attached to the upper and lower surfaces of the vacuum chamber. The trim coils are circular current loops, centred on the cyclotron centre, that change the field slightly around the coil such that the radial gradient of the average field $\frac{\partial \overline{B}(R)}{\partial R}$, achieves its largest value at the radius of the coil. The harmonic coils are provided in sets of 6; one for each pole piece. The area of the closed loop is contained in a radial; interval so that the field under a pole piece will be changed between the inner and outer radii.

54 Trim coils are needed to provide separated turn acceleration[17]; this number is the minimum required to control the radial gradient of the field to $\pm$ 1g./ft. Initially, it was planned to only provide power supplies for 35 of these coils; which will enable us to tune the field to $\pm$ 2 g./ft.[18] There are harmonic coil pairs for each 60^{o} sector; they are required to produce a $\pm$ 7.5 g./pair field bump.

Measurements of a few of these coils were made on the 1/20 scale model of the cyclotron magnet.[19] The results indicated that the coils were more efficient than previously anticipated. It was decided to install some of these coils in the 1/10 scale model to check the efficiencies of the coils and verify that they could perform as required. The information obtained was needed to determine the power supply requirements and conductor requirements. Also, in the full scale survey, it is desirable if the characteristics of a few of the coils are measured in detail and that the fields of the remainder can be interpolated from these. To test this possibility, we needed more data than was available from the 1/20 scale model measurements.

5.1.2 Measurement System

Two aluminum plates, approximately 65 in. in diameter, were prepared so that they could be mounted on the pole surfaces of the 1/10 scale model. Holes were drilled in these plates and the coils tied to the plate by means of these. The coils were made of 1/8 in. copper tubing covered with heat shrink tubing. They were water cooled. Table 5.1 lists the coils that were installed in this magnet along with the corresponding number in the full scale magnet, and their full scale radii. R_I and R_O are the inside and outside radii respectively of the harmonic coils.

TRIM COILS			HARMONIC COILS			
No.	Main Magnet No.	Radius (in.)	No.	Main Magnet No.	R_I (in.)	R_O (in.)
1	T3	27.	1	H2	37.	55.
2	T4	33.5	2	H3	55.	71.
3	T5	40.	3	H4	71.	89.
4	T6	46.5	4	H5	89.	115.
5	T10	72.5	5	H7	141.	167.
6	T14	98.5	6	H9	190.	220.
7	T18	124.5	7	H11	246.	271.5
8	T22	150.5	8	H13	297.	323.
9	T26	176.				
10	T30	200.				
11	T34	224.				
12	T38	248.				
13	T42	270.				
14	T45	285.				
15	T46	290.				
16	T47	295.				
17	T48	300.				
18	T49	304.				
19	T51	312.				
20	T54	325.				

Table 5.1. Trim and harmonic coils installed in the 1/10 scale magnet model.

The trim coils were wound in complete 360° circles. Deviations from the true radius were, at most, 0.1 in. and usually much less. The harmonic coils were placed under 3 pole pieces in the region of our surveys. All the coils were connected in series; the trim coils were excited with 100 amperes and the harmonic coils by 50 amperes. The current supply being regulated to only 1%. In every case measurements were made over a 180° azimuthal range; the radial increments were varied to suit the individual measurements, being closer near the coil and spaced apart more away from the coil. To measure the effect of these coils a survey was made with and without a coil excited, and the difference of the fields examined. The field values reported are the radial averages of the difference field.

5.2 Trim Coils

Table 5.2 summarizes the results of the effect of individual trim coils. R_0 is the radius at which the field passes through zero. All quantities have been scaled to full size; so $\frac{\text{grad.}}{AT}$ is $\frac{d\bar{B}}{dR}$, in gauss/ft., divided by the full scale ampere-turns, which is 2000 for the trim coils.

Because there was noise in the data of about 1 to 2 gauss, and because the data had to be interpolated to provide values every 5 in. from 0. to 325. in.; the

POSITIVE CURRENT						NEGATIVE CURRENT				
TRIM COIL	B max (g.)	B min (g.)	R_0 (in.)	$\frac{d\bar{B}}{dR}$ @ R_0 (g./ft.)	$\frac{\text{grad.}}{AT}$ (g./ft.) AT.	B min (g.)	B max (g.)	R_0 (in.)	$\frac{d\bar{B}}{dR}$ @ R_0 (g./ft.)	$\frac{\text{grad.}}{AT}$ (g./ft.) AT.
T3	27.	- 3.	34.	-23.	.011	-26.	3.	34.	23.	.011
T5	26.	- 3.	44.	-23.	.011	-25.	4.	44.	26.	.013
T6	23.	- 3.	50.	-23.	.011	-23.	4.	50.	24.	.012
T10	23.	- 5.	78.	-23.	.011	-29.	7.	78.	23.	.011
T14	23.	- 7.	103.5	-25.	.013	-22.	7.	103.5	24.	.012
T18	24.	- 9.	128.	-29.	.014	-23.	9.	128.	29.	.014
T22	20.	- 9.	152.	-24.	.012	-21.	8.	153.	28.	.014
T26	21.	- 9.	179.	-26.	.013	-21.	9.	179.	25.	.013
T30	20.	-11.	202.5	-29.	.014	-22.	10.	203.	25.	.013
T34	20.	-11.	230.	-26.	.013	-19.	11.	230.	28.	.014
T38	18.	-12.	250.	-24.	.012	-19.	12.	250.	24.	.012
T42	18.	-14.	271.	-29.	.014	-19.	14.	271.	28.	.014
T46	17.5	-16.	290.	-20.4	.010	-17.	15.	290.	20.4	.010
T47	17.	-17.	295.	-20.4	.010	-17.	17.	295.	20.4	.010
T48	15.	-21.	300.	-19.	.010	-20.	11.	301.	28.	.014
T49	16.	-17.	303.	-23.	.011	-16.	17.	303.	23.	.011
T51	16.	-18.	312.	-28.	.014	-16.	18.	312.	29.	.014
T54	14.	- 3.	324.	-20.4	.010	-14.	2.	324.5	19.	.010

Table 5.2. Trim coil characteristics.

results for each trim coil field were fitted with cubic splines[20]. Cubic splines are polynomials of degree 3 having continuous first and second derivatives at their end points or knots. Several splines, the number being specified by the programmer, were used to fit the data. Their end points are initially specified by the user but are changed by the program to provide some minimization of the least square error. For this work, 4 to 8 splines were used to fit the data over the 325. in range. Fig. 5.1 gives a typical sample of the spline fit compared to the data. In no case was the difference between a data point and the derived spline value more than 2 gauss. Table 5.3 and table 5.4 summarize the results of our measurements, for positive and negative currents respectively, as expressed by means of the coefficients of the splines used. The 4 coefficients A(I) are those needed to describe the cubic that fits the data from one knot to the next; R-KNOT being the knot radii, and where

$$B = A_1 + A_2R + A_3R^2 + A_4R^3 \qquad (5.1)$$

Fig. 5.2 is a contour plot of 18 of the trim coils measured, each having 200 ampere-turns excitation in the 1/10 scale model. The crosses on the vertical axis indicate the position of the trim coils. The contours are labelled by their field values; they are separated by 4 gauss. The zigzaggedness of the ridge of high gradient is a consequence of the contour routine and

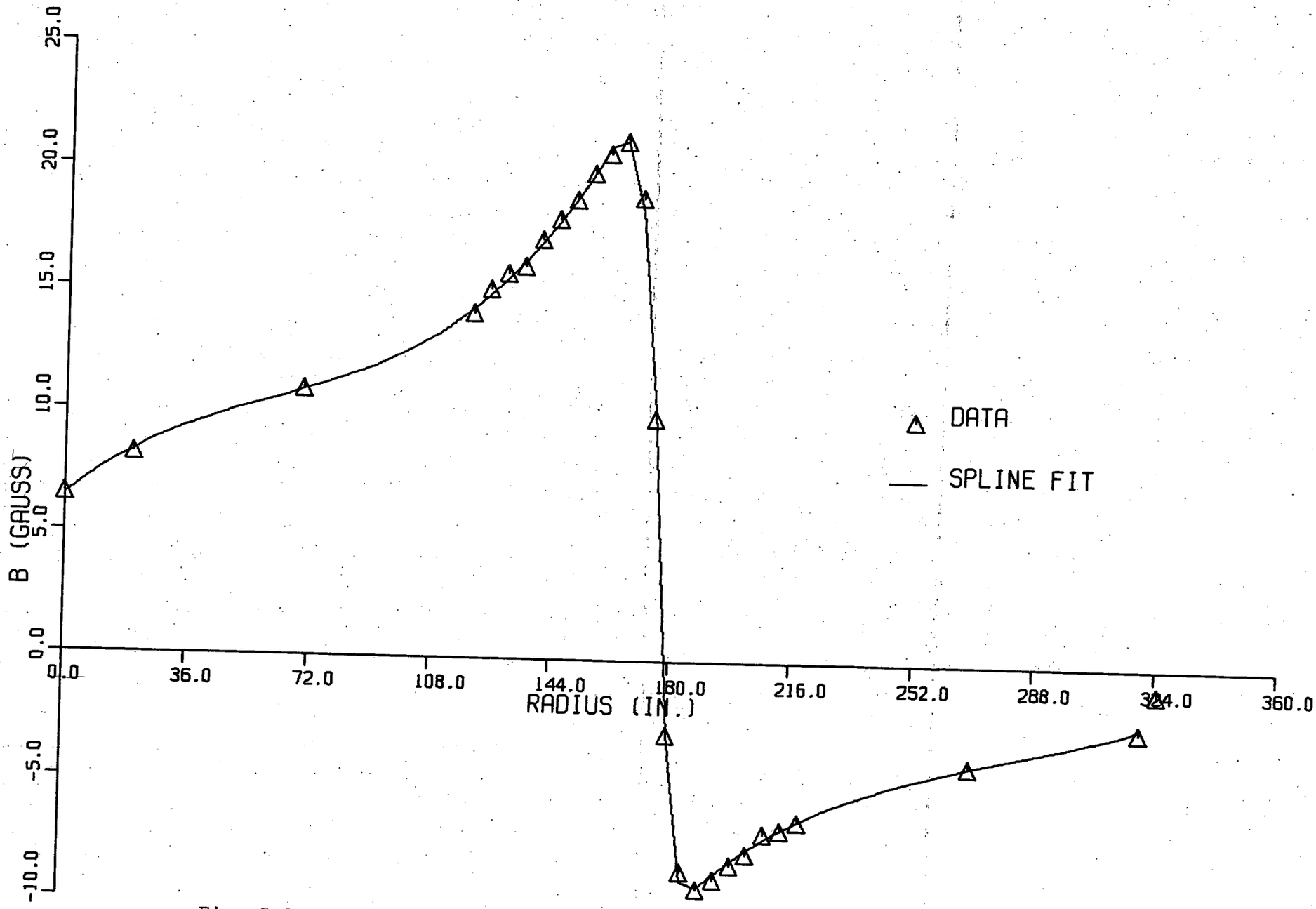

Fig. 5.1. Typical trim coil data with spline fit.

Table 5.3 Coefficients of spline fits used for smoothing and interpolating the trim coil results. This is the case for positive 200 ampere-turn excitation.

NO.	R-KNOT	A(1) (kg.)	A(2) (kg./in.)	A(3) (kg./in.^{2})	A(4) (kg./in.^{3})
T3	0.000	0.240260E-01	0.143612E-02	-0.109454E-03	0.145676E-05
	35.956	0.187477E-02	-0.784889E-03	0.476838E-04	-0.910373E-06
	53.537	-0.213281E-02	0.476044E-04	-0.330619E-06	0.683499E-09
	325.000				
T5	0.000	0.265797E-01	-0.954049E-03	0.756371E-04	-0.159072E-05
	36.886	0.144666E-01	-0.186702E-02	-0.100384E-03	0.113815E-04
	45.278	-0.154414E-02	-0.114744E-02	0.186137E-03	-0.873898E-05
	52.612	-0.339480E-02	0.172670E-03	-0.615600E-05	0.787671E-07
	78.708	-0.168126E-02	0.122972E-04	0.105474E-07	-0.140341E-09
	325.000				
T6	0.000	0.209023E-01	0.162454E-03	-0.181036E-04	0.535069E-06
	24.369	0.218536E-01	0.233368E-03	0.210086E-04	-0.295207E-05
	43.038	0.143251E-01	-0.206876E-02	-0.144329E-03	0.220005E-04
	47.785	0.360471E-02	-0.195157E-02	0.169008E-03	-0.454870E-05
	60.471	-0.324041E-02	0.140377E-03	-0.410215E-05	0.676119E-07
	77.151	-0.172644E-02	0.599625E-04	-0.718817E-06	0.297762E-08
	117.717	-0.278112E-03	0.163435E-04	-0.356465E-06	0.190401E-08
	199.169	-0.282938E-03	-0.382997E-05	0.108818E-06	-0.603922E-09
	325.000				
T10	0.000	0.174039E-01	-0.363905E-03	0.210447E-04	-0.245860E-06
	66.697	0.138026E-01	-0.837799E-03	-0.281499E-04	0.146112E-05
	81.606	-0.102955E-03	-0.702868E-03	0.372004E-04	-0.571970E-06
	103.823	-0.362897E-02	0.103130E-03	-0.921787E-06	0.240057E-08
	325.000				
T14	0.000	0.973331E-02	0.369499E-03	-0.862102E-05	0.775336E-07
	72.106	0.206205E-01	0.335592E-03	0.815104E-05	-0.139284E-05
	95.834	0.145657E-01	-0.163012E-02	-0.909934E-04	0.818032E-05
	104.102	-0.510266E-03	-0.145698E-02	0.111936E-03	-0.263865E-05
	118.362	-0.617589E-02	0.125732E-03	-0.972775E-06	0.239403E-08
	325.000				
T18	0.000	0.130007E-01	0.111549E-03	-0.166743E-05	0.140937E-07
	107.700	0.232799E-01	0.242814E-03	0.288699E-05	-0.427580E-05
	121.514	0.159129E-01	-0.212537E-02	-0.174317E-03	0.170242E-04
	128.463	-0.156188E-02	-0.208168E-02	0.180601E-03	-0.488809E-05
	140.844	-0.892805E-02	0.142196E-06	-0.946218E-06	0.222190E-08
	325.000				
T22	0.000	0.100101E-01	0.293422E-04	0.107520E-06	0.164135E-08
	114.169	0.172041E-01	0.118076E-03	0.667996E-06	0.280299E-07
	134.471	0.201112E-01	0.179859E-03	0.237946E-05	-0.475375E-05
	145.828	0.154977E-01	-0.160544E-02	-0.159567E-03	0.120440E-04
	154.433	-0.245922E-02	-0.167600E-02	0.151375E-03	-0.423756E-05
	166.420	-0.809743E-02	0.126392E-03	-0.101266E-05	0.301571E-08
	325.000				
T26	0.000	0.638026E-02	0.116541E-03	-0.122207E-05	0.665394E-08
	158.039	0.205400E-01	0.228842E-03	0.190975E-05	-0.301601E-05
	175.000	0.808503E-02	-0.258527E-02	-0.159291E-03	0.329404E-04
	179.974	-0.289375E-02	-0.223646E-02	0.244943E-03	-0.849347E-05
	189.624	-0.929829E-02	0.118115E-03	-0.953412E-06	0.344405E-08
	325.000				
T30	0.000	0.698528E-02	0.235194E-03	-0.307146E-04	0.114486E-05
	9.257	0.743866E-02	-0.391401E-04	0.106750E-05	-0.277453E-08
	112.240	0.116990E-01	0.924529E-04	0.210226E-06	0.254980E-09
	189.016	0.201517E-01	0.129243E-03	0.268467E-06	-0.133344E-04
	196.281	0.159907E-01	-0.197856E-02	-0.290377E-03	0.263960E-04

No.	R-Knot	A(1)	A(2)	A(3)	A(4)
	202.593	-0.142747E-02	-0.248958E-02	0.209411E-03	-0.531958E-05
	216.492	-0.985884E-02	0.248663E-03	-0.124092E-04	0.283734E-06
	230.744	-0.801412E-02	0.678469E-04	-0.278861E-06	0.119962E-08
	325.000				
T34	0.000	0.667166E-02	0.444028E-04	-0.405728E-06	0.234604E-08
	206.325	0.191671E-01	0.176592E-03	0.104461E-05	-0.335208E-05
	220.787	0.117999E-01	-0.189652E-02	-0.144394E-03	0.127413E-04
	229.112	-0.664430E-02	-0.165160E-02	0.173813E-03	-0.562350E-05
	239.523	-0.113455E-01	0.138963E-03	-0.182381E-05	0.140228E-07
	325.000				
T38	0.000	0.500385E-02	0.103711E-03	-0.275401E-05	0.211372E-07
	53.268	0.590369E-02	-0.976062E-05	0.623770E-06	-0.115011E-08
	233.629	0.176917E-01	0.103007E-03	0.131386E-09	-0.529809E-05
	245.259	0.105566E-01	-0.204661E-02	-0.184840E-03	0.181029E-04
	252.787	-0.760189E-02	-0.175193E-02	0.223991E-03	-0.933635E-05
	260.743	-0.120639E-01	0.392960E-04	0.114046E-05	-0.843734E-08
	325.000				
T42	0.000	0.605391E-02	-0.866356E-05	0.583609E-07	0.686501E-09
	252.341	0.186147E-01	0.151931E-06	0.578037E-06	-0.344238E-05
	268.914	0.562169E-02	-0.266540E-02	-0.170552E-03	0.325837E-04
	272.994	-0.588000E-02	-0.242975E-02	0.228326E-03	-0.697948E-05
	283.856	-0.142778E-01	0.600243E-04	0.891083E-06	0.177173E-08
	325.000				
T46	0.000	0.489685E-02	-0.110594E-04	0.117868E-06	0.221082E-09
	202.531	0.932846E-02	0.638902E-04	0.252893E-06	0.157936E-07
	216.033	0.102761E-01	0.793572E-04	0.893336E-06	-0.327530E-08
	272.232	0.169759E-01	0.148735E-03	0.340372E-06	-0.336640E-05
	283.355	0.140393E-01	-0.109325E-02	-0.112002E-03	-0.147036E-04
	286.692	0.859835E-02	-0.233178E-02	-0.259196E-03	0.327512E-04
	291.309	-0.446921E-02	-0.263078E-02	0.194432E-03	-0.463001E-05
	305.541	-0.158753E-01	0.900924E-04	-0.325166E-05	0.168227E-06
	325.000				
T47	0.000	0.298155E-02	0.393247E-04	-0.281937E-06	0.114984E-08
	275.431	0.164501E-01	0.145704E-03	0.668075E-06	-0.264754E-05
	293.307	0.414471E-02	-0.236848E-02	-0.141335E-03	0.246827E-04
	297.208	-0.577940E-02	-0.234443E-02	0.147480E-03	-0.270669E-05
	325.000				
T48	0.000	0.189389E-02	-0.291490E-04	0.484109E-06	-0.100801E-08
	188.471	0.684801E-02	0.459148E-04	-0.858565E-07	0.641362E-08
	278.819	0.150255E-01	0.187460E-03	0.164961E-05	-0.297213E-05
	289.263	0.137777E-01	-0.750587E-03	-0.914725E-04	0.254185E-05
	325.000				
T49	0.000	0.396670E-02	0.125074E-04	-0.137874E-06	0.788354E-09
	238.645	0.981411E-02	0.813957E-04	0.426534E-06	0.131148E-07
	285.750	0.159654E-01	0.208880E-03	0.228287E-05	-0.511534E-05
	293.360	0.154327E-01	-0.645120E-03	-0.114499E-03	0.333541E-05
	325.000				
T51	0.000	0.370028E-02	0.300301E-04	-0.837136E-06	0.545082E-08
	75.437	0.354173E-02	-0.321421E-05	0.396391E-06	-0.148826E-08
	166.677	0.541791E-02	0.319511E-04	-0.109646E-07	0.293327E-08
	277.498	0.128163E-01	0.137593E-03	0.964151E-06	-0.397486E-07
	298.530	0.157669E-01	0.125400E-03	-0.153859E-05	-0.862309E-05
	305.948	0.130980E-01	-0.132110E-02	-0.193442E-03	0.926703E-05
	325.000				
T54	0.000	0.202193E-02	0.191467E-04	-0.164295E-06	0.723777E-09
	293.437	0.117810E-01	0.109690E-03	0.472933E-06	0.138664E-06
	307.526	0.138081E-01	0.205592E-03	0.633411E-05	-0.421630E-05
	325.000				

Table 5.3. Coefficients of spline fits used for smoothing and interpolating the trim coil results. This is thecase for positive 200 a - t excitation.

Table 5.4. Coefficients of spline fits used for smoothing and interpolating the trim coil results. This is case for negative 200 ampere-turn excitation.

NO.	R-KNOT	A(1) (kg.)	A(2) (kg./in.)	A(3) (kg./in.^{2})	A(4) (kg./in.^{3})
T3	0.000	-0.256146E-01	0.305148E-03	-0.603668E-04	0.249794E-05
	24.048	-0.184479E-01	0.173546E-02	0.119839E-03	-0.139897E-04
	29.363	-0.793948E-02	0.182380E-02	-0.103258E-03	0.189178E-05
	47.620	0.245206E-02	-0.548711E-04	0.356054E-06	-0.692752E-09
	325.000				
T5	0.000	-0.205795E-01	0.357036E-03	-0.569862E-04	0.138895E-05
	38.254	-0.125590E-01	0.209490E-02	0.102412E-03	-0.166426E-04
	44.276	0.135679E-03	0.151776E-02	-0.198256E-03	0.796553E-05
	52.628	0.362327E-02	-0.126975E-03	0.132365E-05	-0.408827E-08
	190.829	0.564997E-03	0.463244E-05	-0.371340E-06	0.227055E-08
	325.000				
T6	0.000	-0.208111E-01	0.477636E-03	-0.465544E-04	0.915969E-06
	42.279	-0.146102E-01	0.145299E-02	0.696585E-04	-0.657991E-05
	50.357	-0.179717E-02	0.128965E-02	-0.898442E-04	0.195838E-05
	65.743	0.390968E-02	-0.842229E-04	0.547754E-06	-0.109922E-08
	325.000				
T10	0.000	-0.144846E-01	0.485636E-03	-0.291640E-04	0.325786E-06
	64.932	-0.167232E-01	0.818967E-03	0.342976E-04	-0.140049E-05
	81.120	-0.419199E-03	0.828395E-03	-0.337152E-04	0.399345E-06
	110.082	0.499398E-02	-0.119614E-03	0.982239E-06	-0.250556E-08
	325.000				
T14	0.000	-0.998891E-02	0.539816E-05	-0.438543E-05	0.313259E-07
	83.483	-0.218761E-01	-0.718357E-04	0.345895E-05	0.349151E-05
	96.626	-0.142998E-01	0.182784E-02	0.141104E-03	-0.122586E-04
	106.833	0.602185E-02	0.877003E-03	-0.234260E-03	0.185444E-04
	111.089	0.694067E-02	-0.109300E-03	0.253689E-05	-0.298208E-07
	151.715	0.468777E-02	-0.508274E-04	-0.109760E-05	0.217640E-07
	181.155	0.279545E-02	-0.588643E-04	0.824594E-06	-0.463735E-08
	262.857	0.961342E-03	-0.169884E-04	-0.312094E-06	0.708181E-08
	325.000				
T18	0.000	-0.900017E-02	0.824975E-04	-0.504196E-05	0.283731E-07
	111.565	-0.231529E-01	0.169447E-04	0.445914E-05	0.658722E-05
	122.226	-0.144844E-01	0.235794E-02	0.215110E-03	-0.281143E-04
	127.223	-0.839046E-03	0.240180E-02	-0.206365E-03	0.556182E-05
	139.667	0.781025E-02	-0.150412E-03	0.127338E-05	-0.369159E-08
	325.000				
T22	0.000	-0.399709E-02	-0.160438E-03	0.725753E-06	-0.200118E-08
	81.700	-0.133519E-01	-0.819224E-04	0.235451E-06	-0.240360E-07
	132.985	-0.201761E-01	-0.247426E-03	-0.346016E-05	0.391279E-05
	147.462	-0.126111E-01	0.211259E-02	0.166471E-03	-0.194144E-04
	153.649	0.223347E-02	0.194309E-02	-0.193875E-03	0.603642E-05
	164.406	0.821499E-02	-0.132460E-03	0.938904E-06	-0.249608E-08
	325.000				
T26	0.000	-0.430804E-02	-0.143882E-03	0.112171E-05	-0.537547E-08
	159.153	-0.204649E-01	-0.195313E-03	-0.144879E-05	0.351867E-05
	174.678	-0.106805E-01	0.230387E-02	0.162323E-03	-0.232041E-04
	179.936	0.254863E-02	0.208617E-02	-0.203825E-03	0.625119E-05
	190.854	0.916463E-02	-0.129068E-03	0.926829E-06	-0.256466E-08
	325.000				
T30	0.000	-0.509887E-02	0.157088E-04	-0.204041E-05	0.134998E-07
	105.798	-0.102890E-01	0.372826E-04	0.224417E-05	-0.330230E-06
	113.087	-0.100259E-01	0.173658E-04	-0.497735E-05	0.364682E-07
	181.592	-0.204706E-01	-0.151152E-03	0.252086E-05	0.317077E-05
	194.860	-0.146255E-01	0.159042E-02	0.128739E-03	-0.895168E-05

No.	R-Knot	A(1)	A(2)	A(3)	A(4)
	204.963	0.535197E-02	0.145058E-02	-0.142581E-03	0.450812E-05
	215.154	0.100982E-01	-0.509228E-04	-0.475642E-05	0.724517E-07
	252.664	0.531961E-02	-0.101934E-03	0.339641E-05	-0.341828E-07
	325.000				
T34	0.000	-0.181514E-02	-0.572307E-04	-0.697590E-07	-0.224970E-09
	208.497	-0.188191E-01	-0.115659E-03	-0.208012E-06	0.445756E-05
	222.397	-0.849609E-02	0.246223E-02	0.185664E-03	-0.272580E-04
	227.811	0.595070E-02	0.207573E-02	-0.257064E-03	0.101401E-04
	236.271	0.112526E-01	-0.965690E-04	0.307793E-06	-0.265533E-09
	325.000				
T38	0.000	-0.113989E-02	-0.102100E-03	0.609706E-06	-0.211042E-08
	231.832	-0.183364E-01	-0.159680E-03	-0.858181E-06	0.396350E-05
	247.574	-0.559996E-02	0.276003E-02	0.186331E-03	-0.356797E-04
	252.424	0.809840E-02	0.204970E-02	-0.332788E-03	0.179092E-04
	258.562	0.122832E-01	-0.114108E-04	-0.302677E-05	0.302732E-07
	325.000				
T42	0.000	-0.161744E-02	-0.426557E-04	-0.120554E-07	-0.300884E-09
	253.156	-0.180703E-01	-0.106609E-03	-0.240928E-06	0.365991E-05
	270.033	-0.234419E-02	0.301269E-02	0.184880E-03	-0.102361E-03
	271.378	0.179174E-02	0.295473E-02	-0.228173E-03	0.572663E-05
	284.464	0.142469E-01	-0.750733E-04	-0.335356E-05	0.656866E-07
	325.000				
T46	0.000	-0.240613E-02	0.697302E-05	-0.461979E-06	0.133878E-08
	203.310	-0.883348E-02	-0.148620E-04	0.354610E-06	-0.416388E-07
	255.863	-0.146788E-01	-0.322589E-03	-0.621039E-05	0.100832E-05
	273.894	-0.166037E-01	0.436867E-03	0.483306E-04	-0.937067E-06
	310.000	0.000000E 00	0.000000E 00	0.000000E 00	0.000000E 00
	325.000				
T47	0.000	-0.221625E-02	-0.354405E-04	0.212946E-06	-0.987285E-09
	275.552	-0.164695E-01	-0.142976E-03	-0.602452E-06	0.265311E-05
	293.495	-0.390398E-02	0.239115E-02	0.142206E-03	-0.254470E-04
	297.357	0.601149E-02	0.235750E-02	-0.152629E-03	0.284539E-05
	325.000				
T48	0.000	-0.400711E-02	-0.847376E-04	0.695287E-06	-0.208775E-08
	261.656	-0.159770E-01	-0.149691E-03	-0.944144E-06	-0.937236E-07
	279.099	-0.193729E-01	-0.268186E-03	-0.584902E-05	0.387973E-05
	287.138	-0.198913E-01	0.389931E-03	0.877166E-04	-0.209179E-05
	325.000				
T49	0.000	-0.201091E-02	0.321622E-04	-0.834299E-06	0.274658E-08
	148.263	-0.663056E-02	-0.341037E-04	0.387357E-06	-0.473733E-08
	285.000	-0.161627E-01	-0.193893E-03	-0.155779E-05	0.448695E-05
	293.160	-0.154105E-01	0.677013E-03	0.108283E-03	-0.317743E-05
	325.000				
T51	0.000	-0.240025E-02	0.211928E-04	-0.545776E-06	0.196642E-08
	112.481	-0.412319E-02	-0.269484E-04	0.117910E-06	-0.204091E-08
	159.167	-0.533199E-02	-0.292841E-04	-0.167853E-06	-0.110765E-08
	271.875	-0.123506E-01	-0.109332E-03	-0.542068E-06	-0.784599E-08
	299.481	-0.159471E-01	-0.157200E-03	-0.119512E-05	0.133559E-04
	304.614	-0.149791E-01	0.886249E-03	0.204473E-03	-0.827445E-05
	325.000				
T54	0.000	-0.278674E-02	0.218793E-04	-0.376617E-06	0.988617E-09
	176.704	-0.522552E-02	-0.186136E-04	0.147477E-06	-0.406574E-08
	308.197	-0.143669E-01	-0.190725E-03	-0.145611E-05	0.419391E-05
	325.000				

Table 5.4. Coefficients of spline fits used for smoothing and interpolating the trim coil results. This is case for negative 200 ampere-turn excitation.

Fig. 5.2. Contour plot of 18 measured trim coil fields.

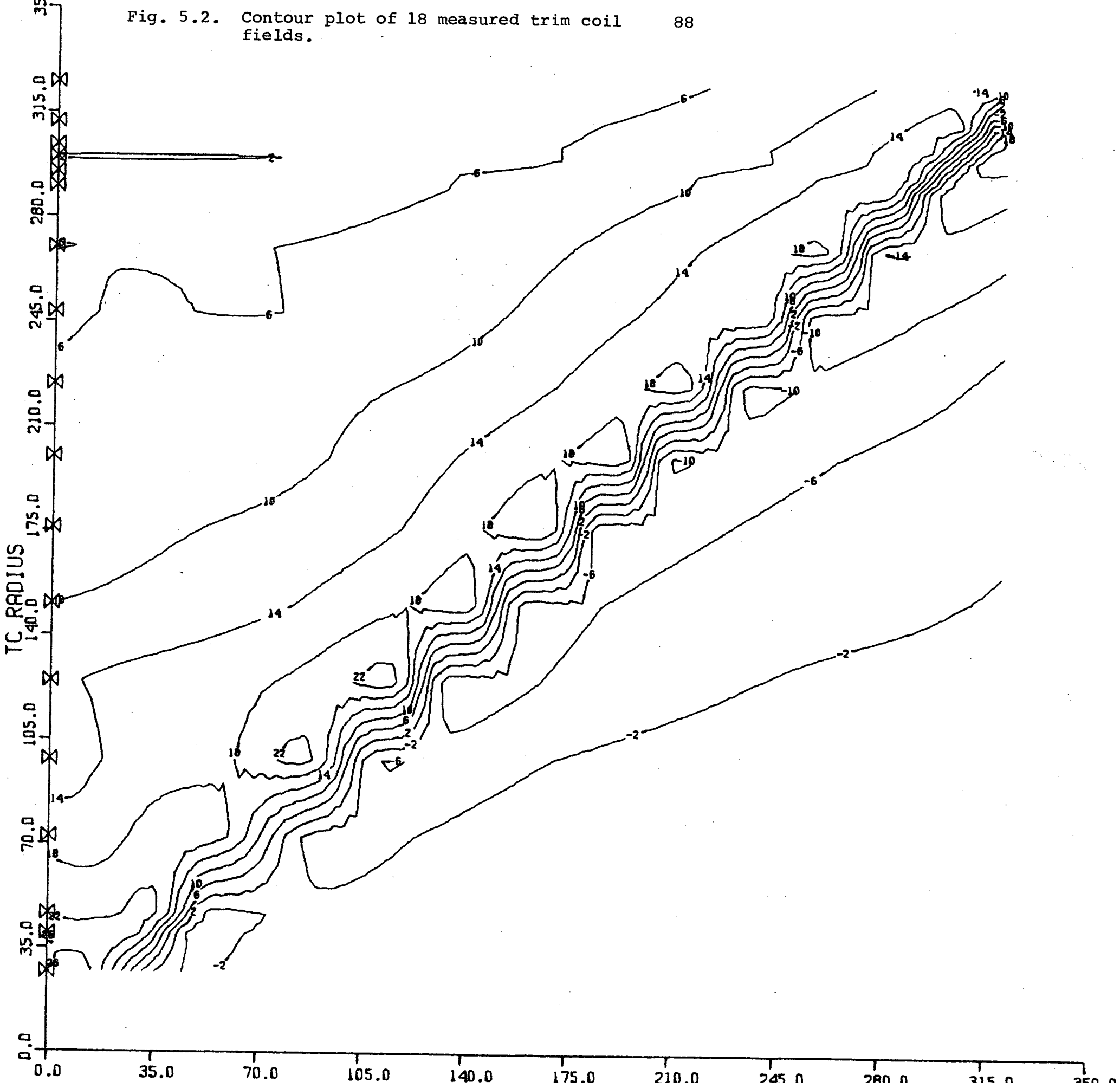

the large radial separation of the coils. Around 300 in. where the coils are close together the contour lines are straighter. The ridge of high gradiant should be straight, with a 45^{o} slope.

It was found that field profiles for positive and negative currents were the same, and that the trim coils produced much the same field at any radius. There was though, a change in the relative values of the maximum inside the coil and outside the coil, as we can see in table 5.2. Also the difference between the coil radius and R_0 changed significantly with radius, cf. table 5.5. And since the trim coil field has its maximum gradient at R_0 this property will affect the choice of trim coil excitations.

Several additional experiments were done to test the superposition of various trim coil fields. Coils T46 and T47 were measured with their fields adding and subtracting in both positive and negative directions. Table 5.6 summarizes the results. The sum columns are for when the fields opposed each other. The calculated sums and differences agree with the measured values within the measurement accuracy.

T45,46,48, and 49 were all powered with 200 ampere-turns each in the same direction. Then the effect of T22 and T47 combined with this group were separately measured.

TRIM COIL	R(in.)	POSITIVE CURRENT $R-R_0$(in.)	NEGATIVE CURRENT $R-R_0$(in.)
T3	27.	-7.	-7.
T5	40.	-4.	-4.
T6	46.5	-3.5	-3.5
T10	72.5	-5.5	-5.5
T14	98.5	-5.	-5.
T18	124.5	-3.5	-3.5
T22	150.5	-1.5	-2.5
T26	176.	-3.0	-3.
T30	200.	-2.5	-3.
T34	224.	-6.	-6.
T38	248.	-2.	-2.
T42	270.	-1.	-1.
T46	290.	-0.	0.
T47	295.	-0.	0.
T48	300.	0.	-1.
T49	304.	1.	1.
T51	312.	0.	0.
T54	325.	1.	0.5

Table 5.5. Variation of the difference between the trim coil radius and R_0 with radius.

R (in.)	ADDITION OF FIELDS SUM +I	SUM -I	DIFFERENCE +-	DIFFERENCE -+	MEASURED FIELDS SUM +I	SUM -I	DIFFERENCE +-	DIFFERENCE -+
50.	9.	- 5.	2.	1.	7.	- 7.	1.	0.
100.	10.	- 9.	0.	0.	9.	- 9.	0.	- 1.
150.	12.	-13.	0.	- 1.	13.	-12.	0.	- 1.
200.	16.	-17.	1.	- 1.	16.	-16.	1.	- 1.
250.	23.	-24.	1.	- 2.	24.	-24.	1.	- 1.
255.	24.	-25.	2.	- 2.	26.	-25.	1.	- 2.
260.	26.	-27.	2.	- 3.	27.	-26.	1.	- 2.
265.	27.	-27.	2.	- 2.	28.	-27.	2.	- 2.
270.	29.	-29.	2.	- 2.	29.	-29.	2.	- 2.
275.	31.	-30.	3.	- 2.	30.	-31.	2.	- 2.
280.	32.	-31.	3.	- 2.	31.	-32.	2.	- 2.
285.	32.	-32.	1.	- 1.	32.	-32.	1.	- 1.
290.	28.	-28.	-5.	3.	28.	-28.	-4.	4.
295.	15.	-15.	-15.	16.	15.	-15.	-15.	15.
300.	-3.	3.	-21.	21.	-3.	2.	-21.	21.
305.	-20.	20.	-12.	12.	-21.	20.	-12.	12.
310.	-31.	31.	-2.	2.	-31.	31.	- 2.	2.
315.	-33.	33.	1.	-1.	-34.	33.	1.	-1.
320.	-33.	32.	1.	-2.	-33.	32.	2.	-2.

Table 5.6. Superposition of fields from trim coils T47 and T49; all field values are in gauss.

They showed clearly that for even such a large group of coils the fields satisfied the principle of superposition.

5.3 Harmonic Trim Coils

The results of these coils, measured independently, are summarized in table 5.7. RO_I and RO_O are the inside and outside respectively radii where the field is zero. B/AT is the maximum field per ampere-turn, in full scale values. Fig. 5.3 illustrates a harmonic coil field.

	POSITIVE CURRENT				NEGATIVE CURRENT			
HARMONIC COIL.	RO_I (in.)	RO_O (in.)	B_{max} (g.)	B/AT (g./AT)	RO_I (in.)	RO_O (in.)	B_{max} (g.)	B/AT (g./AT)
H2	29.	60.	13.	.013	28.	63.	-12.	-.012
H3	49.	75.	12.	.012	46.	79.	-12.	-.012
H4	61.	95.	13.5	.014	59.	99.	-13.	-.013
H5	82.	122.	14.	.014	82.	122.	-14.	-.014
H7	135.	173.	14.	.014	135.	175.	-15.	-.015
H9	185.	225.	14.5	.014	185.	226.	-14.	-.014
H11	240.	277.	13.5	.014	240.	279.	-13.5	-.014
H13	291.	-	13.	.013	292.	-	-12.	-.012

Table 5.7. Characteristics of the harmonic coils.

The B_{max} values are the maximum field values measured. The average field between the two radii of the harmonic coils is approximately 2/3 of B_{max}. This value is more significant in judging the harmonic coil's effect on the beam.

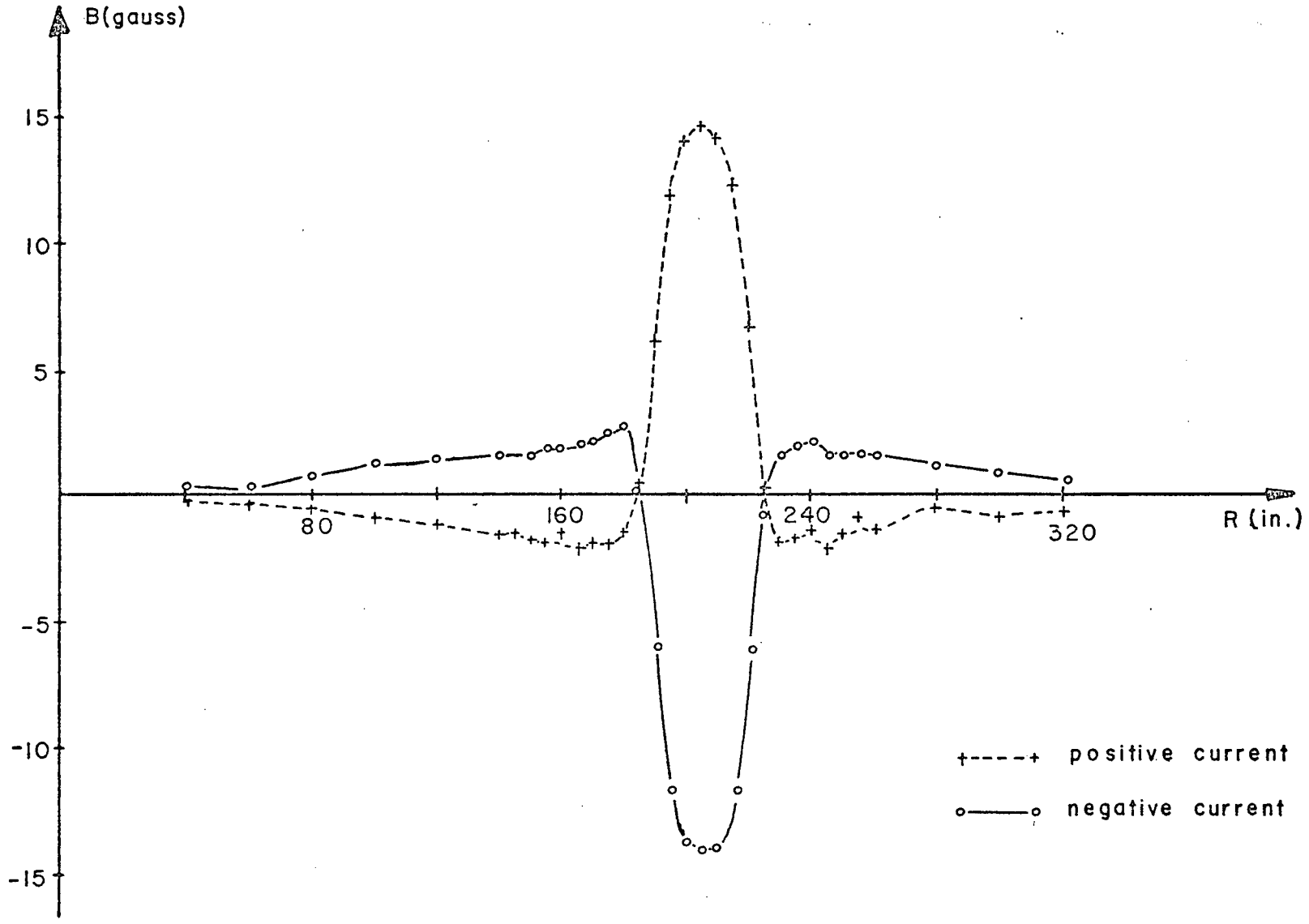

Fig. 5.3. Field of a harmonic coil for ±100 ampere-turns.

The field profiles were the same for both directions of current, and for all the harmonic coils measured. However the radii at which the field was zero again did not correspond exactly to the radii of the coils.

Harmonic coils H2 and H3 were powered so that their fields added and subtracted in both direction; the results are given in table 5.8 along with the expected field based on the principle of superposition.

	ADDITION OF FIELDS				MEASURED FIELDS			
	SUM		DIFFERENCES		SUM		DIFFERENCES	
R (in.)	+I	-I	+-	-+	+I	-I	+-	-+
5.	0.	1.	0.	1.	- 1.	0.	0.	2.
10.	- 1.	1.	0.	0.	- 1.	1.	- 1.	0.
15.	- 1.	1.	- 1.	0.	- 1.	1	- 1.	0.
20.	- 1.	1.	- 1.	1.	- 2.	1.	- 1.	1.
25.	- 1.	2.	- 1.	1.	- 2.	2.	- 1.	1.
30.	0.	0.	1.	- 1.	0.	0.	1.	- 1.
35.	0.	- 5.	6.	- 6.	5.	- 5.	6.	- 6.
40.	10.	-11.	12.	-12.	11.	-10.	12.	-12.
45.	13.	-11.	14.	-12.	12.	-12.	13.	-13.
50.	12.	-12.	9.	- 9.	12.	-12.	9.	- 9.
55.	12.	-11.	- 3.	3.	12.	-11.	- 3.	3.
60.	12.	-13.	-12.	11.	13.	-12.	-12.	12.
65.	10.	-11.	-13.	11.	11.	-12.	-13.	12.
70.	5.	- 6.	- 7.	7.	6.	- 5.	- 7.	7.
75.	- 1.	- 2.	- 3.	0.	- 0.	- 2.	- 2.	2.
80.	- 1.	1.	0.	0.	- 1.	0.	0.	0.
85.	- 1.	1.	0.	0.	- 1.	1.	0.	- 1.
90.	- 2.	0.	- 1.	- 1.	- 1.	1.	0.	- 1.
95.	- 1.	1.	0.	0.	0.	1.	0.	0.
100.	- 1.	1.	0.	0.	- 1.	1.	0.	- 1.
120.	- 1.	1.	0.	0.	- 1.	0.	0.	0.
200.	0.	0.	0.	0.	0.	0.	0.	0.

Table 5.8. Superposition of fields from harmonic coils H2 and H3; all fields are in gauss.

5.4 Other Tests

A half dozen experiments were made testing the superposition of various trim coil and harmonic coils together. Table 5.9 gives one of the results of these measurements; in this sample just the addition of the fields was examined. The law of superposition was satisfied every time within the precision of our measurements.

A measurement was also made of the field of a trim coil when the cyclotron magnet was not excited. The field was the same, within a few gauss, as before.

5.5 Conclusions

The efficiency, as determined by the gradient per ampere-turn, of the trim coils were found to be about 2/3 as much as expected from the 1/20 scale model measurements. But the harmonic coils results agreed with the previous model results. There were no problems as a consequence with the design of the coils.

The coils satisfy their specifications. However allowance will have to be made for the variation of the radii where the maximum gradient is produced by the trim coils. The characteristics of the fields produced were regular enough that it would not be necessary to measure all of them in the full scale magnet.

ADDITION OF FIELDS			MEASURED FIELDS	
RADIUS (in.)	+I	-I	+I	-I
5.	11.	-11.	12.	-11.
10.	10.	-11.	11.	-11.
15.	10.	-10.	11.	-11.
20.	10.	-11.	11.	-11.
25.	11.	-11.	11.	-11.
30.	11.	-11.	12.	-12.
35.	11.	-11.	11.	-11.
40.	9.	- 9.	10.	-10.
45.	5.	- 4.	5.	- 5.
50.	2.	- 1.	1.	- 2.
55.	5.	- 5.	3.	- 4.
60.	10.	-10.	6.	- 7.
65.	11.	-10.	6.	- 6.
70.	5.	- 5.	3.	- 3.
75.	- 1.	- 2.	0.	0.
80.	- 1.	3.	- 1.	1.
85.	- 1.	2.	- 1.	1.
90.	- 1.	1.	- 1.	1.
95.	- 1.	1.	- 1.	1.
100.	- 1.	1.	- 1.	1.

Table 5.9. Superposition of the field from trim coil T6 and harmonic coil H3; all field values are in gauss.

REFERENCES

[1]J.B. Warren, IEEE Trans. Nucl. Sci. N5-18, 272 (1971).

[2]L.P. Robertson, E.G. Auld, G.H. Mackenzie, and A.J. Otter, "Extraction of Multiple Beams of Various Energies From the TRIUMF Negative Ion Isochronous Cyclotron", 5th International Cyclotron Conference (1970).

[3]L.F. Frieson, Master's Thesis (1970).

[4]G.H. Mackenzie, Private communication (1971).

[5]John S. Colonias, "TRIM: A Magnetostatic Computer Program For the CDC 6600", UCRL-18439 (1968).

[6]N.J. Diserns, "TRIM: Users Guide", Rutherford Laboratory (1968).

[7]M.J. Linton, "Main Magnet Code Description", TRI-DN-70-54 (1970).

[8]B. Grey, L.P. Robertson, BCONV, VPN-68-1, (1968).

[9]_____: BFIELD, VPN-68-2, (1968).

[10]L.P. Robertson, Private communication (1972).

[11]G.H. Mackenzie, J.R. Richardson, "A Method for Locating the Median Surface of a AVF Cyclotron Magnet", Nuclear Instruments and Methods, 87, 319-322 (1970).

[12]G.H. Mackenzie, C. Meade, TRI-DN-72-10 (1972).

[13]N.K. Abrosimov, V.A. Eliseev, G.A. Ryabov, "Device for the Measurement of the Median Plane Position", A.F. Joffe Physico-Technical Institute, report No. 40, Leningrad (1967).

[14]D.L. Livesey, "Misalignment Errors in Hall Plates", Parts I and II, TRI-DN-71-16 and TRI-DN-71-18 (1971).

[15]Jean Bolduc, Master's Thesis (1972).

[16]C. Kost, "MARELAX2D", TRI-DN-72-2 (1972).

[17]M.K. Craddock, J.R. Richardson, "Magnetic Field Tolerances For a Six-Sector 500 Mev H^- Cyclotron", TRI-67-2 (1967).

References (Cont'd.)

[18]A.J. Otter, "Trim Coil Redesign", TRI-DN-70-56 (1970).

[19]_____: Letter to L.J.P. Tillson and M. Fischer re: "Trim and Harmonic Coil Ampere Turn Requirements," File 54 (1968).

[20]C. Kost, "Nonlinear Cubic Spline Approximation", TRI-DN-72-9 (1972).

APPENDIX A

GENERAL RELATIONSHIPS FOR MAGNETIC FIELDS.

From Maxwell's equations in the absence of currents

$$\nabla \cdot \vec{B} = 0 \qquad (A.1)$$

$$\nabla \times \vec{B} = 0 \qquad (A.2)$$

Then in cartesian coordinates where By is constant

$$\frac{\partial B_z}{\partial z} = -\frac{\partial B_x}{\partial x} \qquad (A.3)$$

$$\frac{\partial B_z}{\partial x} = \frac{\partial B_x}{\partial z} \qquad (A.4)$$

Combining we get

$$\frac{\partial^2 B_z}{\partial z^2} = \frac{\partial^2}{\partial x^2} B_z \qquad (B.5)$$

Another useful relationship is the Taylor series expansion of B_z about $z = 0$.

$$B_z(z) = B_z(o) + z\left(\frac{\partial B_z}{\partial z}\right)_o + \frac{z^2}{2}\left(\frac{\partial^2 B_z}{\partial z^2}\right)_o + \frac{z^3}{3!}\left(\frac{\partial^3 B_z}{\partial z^3}\right)_o + \cdots \qquad (A.6)$$